NRIM SR-95-02

# Effect of S, REM and $Y_2O_3$ on High Temperature Protective Film

by

Yuji IKEDA

NRIM Special Report
(Research Report)
No. 95–02

1995

National Research Institute for Metals
1–2–1, Sengen, Tsukuba-shi, Ibaraki, Japan

NRIM SR-95-02

# Effect of S, REM and $Y_2O_3$ on High Temperature Protective Film

by

Yuji IKEDA

NRIM Special Report
(Research Report)
No. 95–02

1995

National Research Institute for Metals
1–2–1, Sengen, Tsukuba-shi, Ibaraki, Japan

# Effect of S, REM and $Y_2O_3$ on High Temperature Protective Film

by
Yuji IKEDA

NRIM Special Report
(Research Report)
No. 95–02

## Contents

# Effect of S, REM and $Y_2O_3$ on High Temperature Protective Film

by

Yuji IKEDA

**Abstract**

Since many years the mechanism of high temperature oxidation has been discussed without reaching a very clear-cut conclusion because of the complexity of factors controlling the mechanism, especially those controlling spalling of protective film. In this work oxide coating films made under the same conditions were used as a simulation of oxide scale to avoid the complexity arising from a wide variety of oxide scale features. An important factor "detrimental effect of S" was successfully extracted from others. The results show that S promotes the spalling of a protective film through weakening the bond between the film and substrate alloy. Beneficial effects of rare earth metal (REM) addition and $Y_2O_3$ dispersion on oxidation resistance were systematically explained in terms of the S effect. Spalling characteristics of protective films were compared between REM addition and $Y_2O_3$ dispersion, $Y_2O_3$ dispersion and other oxides, films on ferritic and austenitic alloys, and mechanical alloying and casting. Although both REM and $Y_2O_3$ improve oxidation resistance, the effect of $Y_2O_3$ dispersion has greater diversity than REM addition. REM and $Y_2O_3$ suppress somewhat differently the diffusion of alloying elements in coating film.

***Keywords:*** *high temperature oxidation, sulfur, rare earth metal, $Y_2O_3$, ODS alloy, surface segregation, oxide coating, spalling of oxide film, diffusion in oxide coating film*

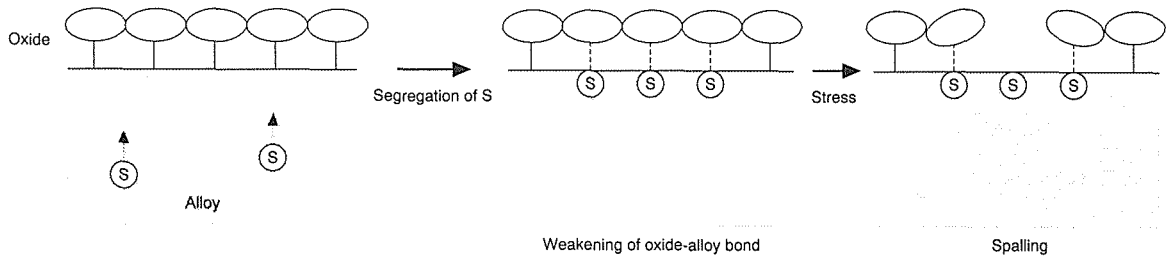


**Fig. 1 Schematic presentation of "detrimental effect of S" model**

## 1. Introduction

Oxidation resistance is an important characteristic of high temperature alloys. The resistance is improved through (1) suppression of cracking and spalling of oxide scale, and (2) suppression of diffusion of alloy or gas components through the scale. Although the first is more important than the second, the hitherto numerous researches do not completely elucidate the factors controlling the cracking and spalling. Many factors have been discussed;

1) Kirkendall void: Interfacial voids reduce net adherent area and promote the spalling.
2) Pegging: Oxide pegs suppress the spalling.
3) Growth stress: Stresses induced during scale growth promote the spalling.
4) Difference in thermal expansion coefficient between oxide and alloy: Thermal cycle produces a large stress owing to the difference in expansion coefficient and hence promote the spalling.
5) Plasticity of oxide: Large plasticity of oxide facilitates the deformation and hence releases the stress.

In NRIM "detrimental effect of S" model was proposed as a new factor[1]. It was found that the extent of spalling increased with increasing S segregation rate to alloy surface. It is reasonably considered in analogy with grain boundary embrittlement by S that S promotes the spalling through interfacial embrittlement (Fig. 1).

Although some of these factors are plausible, there is no definitive evidence with regard to the subject which factors govern spalling characteristics. This is attributed to a wide variety of factors as stated above. Several factors may work simultaneously. One factor may be concurrently of advantage and disadvantage for spalling suppression. For example, interfacial voids reduce the adherent area, but possibly suppress the spalling by facilitating the plastic deformation of the oxide.

On the other hand, coatings applied under the same conditions should have the very similar features on any substrate alloys. Accordingly a factor controlling the spalling of coating film can be examined without being disturbed by others, and the result will be a very important clue, or probably definitive evidence, in elucidating the spalling characteristics of oxide scale.

Since many years it is well known that rare earth metals (REM) improve extensively oxidation resistance of metallic materials. But a very clear-cut explanation has not been given for the mechanism of the improvement, although moderately persuasive models are proposed. This is also the case for the improvement through $Y_2O_3$ dispersion. This work was made to give a systematic explanation for the promotion and suppression of spalling in terms of the detrimental effect of S.

## 2. Experimental

### 2.1 Sample

Six series of alloys were used; commercial stainless steels, type 304 stainless steels with different S content, various stainless steels doped with REM (Table 1), commercial ODS alloys, ferritic ODS alloys and austenitic ODS alloys (Table 2). The dispersion-free alloys were generally rolled, annealed in Ar or vacuum at 1373 K for 7.2 ks (2 h) and cut into coupons of about 10 × 10 × 1 mm. The coupons were ground with emery paper for cyclic oxidation test, and then polished with diamond slurry for surface segregation measurement and spalling experiment of $Al_2O_3$ coating film. The coupons were washed with alcohol and/or hot acetone. The ODS alloys were prepared through mechanical alloying and extrusion, and similar coupons were prepared in a similar manner as above.

**Table 1 Chemical composition of dispersion-free alloys (mass%)**

| Alloy | C | Si | Mn | P | S | Ni | Cr | Ti | Other | Fe |
|---|---|---|---|---|---|---|---|---|---|---|
| Commercial | | | | | | | | | | |
| Type 304-A | 0.070 | 0.51 | 0.99 | 0.033 | 0.008 | 8.60 | 18.12 | – | | Bal. |
| Type 304-B | 0.07 | 0.47 | 0.83 | 0.029 | 0.007 | 8.65 | 18.14 | – | | |
| Type 304-C | 0.08 | 0.34 | 1.08 | 0.027 | 0.013 | 8.9 | 18.7 | – | | |
| Type 304-D | 0.063 | 0.55 | 0.92 | 0.031 | 0.005 | 8.79 | 18.61 | – | | |
| Type 304-E | 0.013 | 0.34 | 1.18 | 0.030 | 0.013 | 8.86 | 19.08 | – | | |
| Type 304-F | 0.059 | 0.57 | 1.83 | 0.033 | 0.009 | 9.02 | 18.90 | – | | |
| Type 321-A | 0.037 | 0.81 | 0.93 | 0.033 | 0.006 | 9.18 | 17.29 | 0.42 | | |
| Type 321 | 0.054 | 0.57 | 1.06 | 0.036 | 0.005 | 9.91 | 17.3 | 0.42 | | |
| Type 347 | 0.061 | 0.57 | 1.75 | 0.020 | 0.003 | 11.19 | 17.40 | – | Nb = 0.87 | |
| Different S content | | | | | | | | | | |
| Type 304-10S | 0.04 | 0.56 | 1.49 | 0.022 | 0.001 | 9.39 | 18.83 | – | | Bal. |
| Type 304-97S | 0.06 | 0.50 | 1.48 | 0.024 | 0.0097 | 10.07 | 18.53 | – | | |
| Type 304-181S | 0.06 | 0.50 | 1.48 | 0.025 | 0.0181 | 10.04 | 18.49 | – | | |
| Doped with REM | | | | | | | | | | |
| Type 310S | 0.04 | 0.94 | 1.68 | 0.030 | 0.007 | 19.99 | 24.79 | – | | Bal. |
| Type 310S-0.1La | 0.064 | 0.59 | 1.03 | 0.019 | 0.011 | 20.1 | 25.6 | – | La = 0.102 | |
| Type 310S-0.15La | 0.064 | 0.62 | 1.09 | 0.019 | 0.003 | 20.0 | 25.5 | – | La = 0.150 | |
| Type 310S-0.05MM[(a)] | 0.060 | 0.61 | 1.05 | 0.022 | 0.035 | 20.0 | 25.9 | – | MM = 0.048 | |
| Type 310S-0.1MM[(a)] | 0.061 | 0.57 | 1.03 | 0.018 | 0.021 | 20.0 | 25.9 | – | MM = 0.106 | |
| Type 310S-0.18MM[(a)] | 0.072 | 0.60 | 1.02 | 0.020 | 0.016 | 20.1 | 25.2 | – | MM = 0.175 | |
| Type 304-Ce | 0.058 | 0.47 | 1.57 | 0.008 | 0.0012 | 9.30 | 18.98 | – | Ce = 0.06 | |
| Type 321-Ce | 0.023 | 0.50 | 1.59 | 0.005 | 0.0024 | 12.52 | 17.95 | 0.75 | Ce = 0.033 | |
| Fe-20Cr-32Ni-0.05Ce | 0.036 | 2.28 | 0.25 | 0.011 | 0.004 | 32.29 | 20.05 | – | Ce = 0.05 | |
| Type 304-BN[(b)] | 0.054 | 0.30 | 1.05 | 0.020 | 0.007 | 8.47 | 19.47 | – | B = 0.01, N = 0.160 | |

(a) MM = misch metal (70%Ce-30%La)

(b) Boron nitride precipitates at the surface and suppresses S segregation.

**Table 2 Chemical composition of ODS alloys (mass%)**

| Alloy | C | Si | Mn | P | S | Fe | Ni | Co | Cr | Al | Ti | Mo | $Y_2O_3$ | $Al_2O_3$ | Other |
|---|---|---|---|---|---|---|---|---|---|---|---|---|---|---|---|
| Commercial | | | | | | | | | | | | | | | |
| MA957 | 0.014 | 0.04 | 0.08 | 0.005 | 0.006 | Bal. | 0.11 | 0.04 | 14.16 | – | 1.02 | 0.31 | 0.27 | – | |
| MA956 | 0.018 | 0.10 | 0.093 | 0.007 | 0.004 | Bal. | – | – | 19.76 | 4.60 | 0.37 | – | 0.52 | – | |
| MA754 | 0.05 | – | 0.002 | 0.002 | 0.001 | 0.33 | Bal. | – | 19.55 | 0.33 | 0.46 | – | 0.57 | – | |
| MA758 | 0.05 | – | 0.004 | 0.002 | 0.001 | 0.67 | Bal. | – | 29.32 | 0.25 | 0.47 | – | 0.6 | – | |
| MA6000 | 0.08 | 0.03 | 0.01 | 0.005 | 0.006 | – | Bal. | – | 14.9 | 4.09 | 2.25 | 2.01 | 1.1 | – | W = 4.14, Ta = 1.69 |
| TMO-2[a] | 0.05 | – | – | 0.005 | 0.003 | – | 58.4 | 9.7 | 5.9 | 4.2 | 0.8 | 2.0 | 1.1 | – | W = 12.4, Ta = 4.7 |
| 304-$Y_2O_3$[b] | – | – | – | – | – | – | – | – | – | – | – | – | 3.0 | – | |
| Ferritic | | | | | | | | | | | | | | | |
| Fe-20Cr-0Y | 0.052 | 0.058 | 0.067 | 0.002 | 0.006 | Bal. | – | 0.008 | 19.08 | 0.065 | – | – | – | – | |
| Fe-20Cr-3Y | 0.042 | 0.057 | 0.056 | 0.002 | 0.006 | Bal. | – | 0.002 | 19.21 | 0.094 | – | – | 0.29 | – | |
| Fe-20Cr-4Y | 0.034 | 0.057 | 0.056 | 0.003 | 0.006 | Bal. | – | 0.006 | 19.31 | 0.10 | – | – | 0.38 | – | |
| Fe-20Cr-6Y | 0.044 | 0.056 | 0.063 | 0.003 | 0.005 | Bal. | – | 0.005 | 18.91 | 0.092 | – | – | 0.57 | – | |
| Fe-20Cr-10Y | 0.045 | 0.054 | 0.066 | 0.003 | 0.006 | Bal. | – | 0.006 | 18.94 | 0.13 | – | – | 0.98 | – | |
| Fe-20Cr-5A | 0.039 | 0.083 | 0.077 | 0.003 | 0.006 | Bal. | – | 0.006 | 18.95 | 0.28 | – | – | – | 0.53 | |
| Fe-20Cr-9S | 0.051 | 0.41 | 0.069 | 0.003 | 0.007 | Bal. | – | 0.005 | 20.70 | 0.078 | – | – | – | – | $SiO_2$ = 0.88[c] |
| Fe-20Cr-8Z | 0.040 | 0.060 | 0.070 | 0.003 | 0.008 | Bal. | – | 0.005 | 19.28 | 0.18 | – | – | – | – | $ZrO_2$ = 0.77[c] |
| Fe-20Cr-YA | 0.044 | 0.053 | 0.063 | 0.003 | 0.006 | Bal. | – | 0.005 | 19.12 | 0.16 | – | – | 0.70 | 0.30 | |
| Austenitic | | | | | | | | | | | | | | | |
| Type 316L[d] | 0.007 | 0.33 | 0.79 | 0.028 | 0.016 | Bal. | 12.13 | – | 16.24 | – | – | 2.02 | – | – | |
| Type 316-1A | 0.064 | 0.62 | 1.18 | 0.019 | 0.014 | Bal. | 11.1[e] | – | 16.9[e] | – | – | 2.13[e] | – | 1 vol%[f] | |
| Type 316-2A | 0.063 | 0.64 | 0.99 | 0.017 | 0.014 | Bal. | 11.1[e] | – | 16.9[e] | – | – | 2.13[e] | – | 2 vol%[f] | |
| Type 316-1Y | 0.043 | 0.62 | 1.25 | 0.025 | 0.011 | Bal. | 11.1[e] | – | 16.9[e] | – | – | 2.13[e] | 1 vol%[f] | – | |
| Type 316-2Y | 0.060 | 0.61 | 1.03 | 0.024 | 0.014 | Bal. | 11.1[e] | – | 16.9[e] | – | – | 2.13[e] | 2 vol%[f] | – | |

(a) Superalloy developed by NRIM.
(b) Sintered.
(c) Calculated from the concentration of Si and Zr.
(d) Cast steel.
(e) Concentration of the starting material.
(f) Added quantity.

**Table 3 $Al_2O_3$ depositing condition**

| | |
|---|---|
| Target | Sintered $Al_2O_3$ (99.9%, 50 mm $\phi$) |
| Sputter gas | Ar (99.999%) |
| RF power density | 51 $kW \cdot tm^{-2}$ |
| Ar sputtering pressure | 0.5 Pa |
| Substrate temperature | Ambient |
| Sputtering time | 7.2 ks |
| Film thickness | *ca.* 2 $\mu$m |

## 2.2 Surface Segregation[1]

A polished sample was inserted into an Auger Electron Spectroscopy system (AES). After surface cleaning by Ar ion sputtering, the sample was heated at 1100 K and the surface concentration was followed for 86.4 ks (24 h). The heating was made through electron bombardment on the back side of the sample.

## 2.3 Cyclic Oxidation[1]

At first the extent of oxide scale spalling was examined on stainless steel samples ground with emery paper through cyclic oxidation test. One cycle consisted of 70 ks (19.5 h) of heating in $O_2$ at 1100 K and cooling at R.T. for type 304, 304-BN, 321 and 347 steels, 10.8 ks (3 h) of heating in $O_2$ at 1273 K and cooling at R.T. for type 304 and 304-BN steels, and 70 ks of heating in air at 1450 K and cooling at R.T. for type 310S steels. The mass change was followed with microbalance at each cycle.

## 2.4 Oxide Coating

Coating was made by magnetron sputtering method under conditions in Table 3.

## 3. Surface Segregation of S and Cyclic Oxidation[1]

### 3.1 Promotion of Spalling by S and Trapping of S by REM

The surface segregation of S was measured at 1000 K on commercial stainless steels and BN doped one. The segregation is very rapid on type 304 steel without doping, very slow on the BN doped, and intermediate on the other two (Fig. 2). The S is enriched to about 20 at% at the very surface of the 304 steel without doping. Thus the scale spalling during cyclic oxidation was expected to

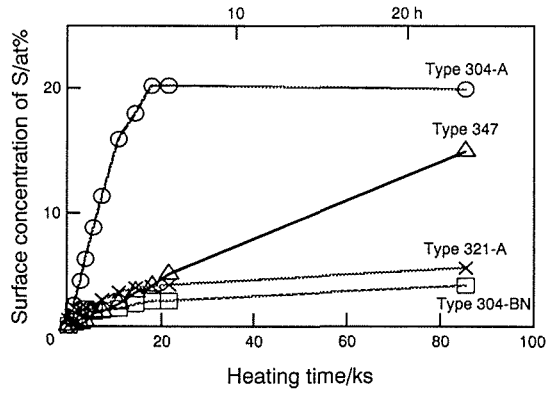


**Fig. 2 Surface segregation of S on stainless steels at 1000 K**

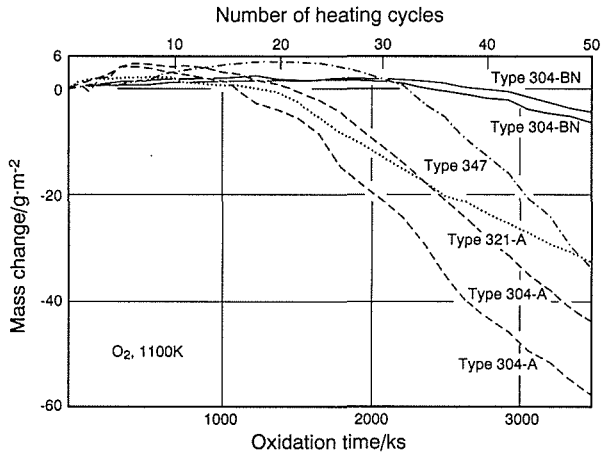


**Fig. 3 Mass change during cyclic oxidation of the same stainless steels as Fig. 2—1 cycle = [heating in $O_2$ at 1100 K for 70 ks (19.5 h)] + [cooling at R.T.]**

be extensive on the 304 steel without doping, suppressed on that doped with BN and intermediate on the other two. Newly ground samples were cyclically oxidized in a stream of $O_2$ purified by silicagel and molecular sieve. The samples were oxidized at 1100 K for 70 ks (about 19.5 h) and weighed at R.T. This oxidation run was repeated up to 50 cycles. The mass change is given in Fig. 3. Completely in accord with the above expectation, the mass loss owing to scale spalling is the largest on the 304 steel without doping, the smallest on the BN doped one and intermediate on the other two.

Similar experiments were made on type 310S steels with and without REM addition. The results are summarized in Fig. 4 with the above results. The abscissa indicates the surface concentration of S after heating for

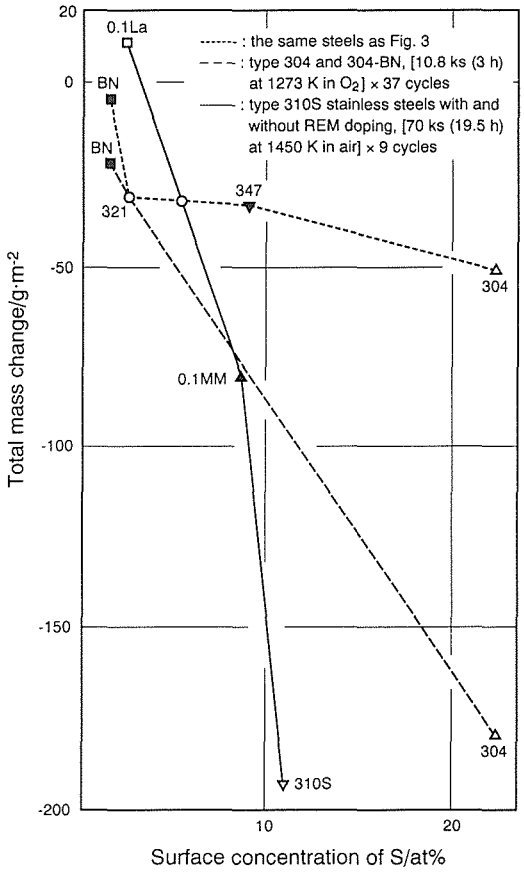


**Fig. 4 Correlation between surface segregation rate of S and mass change during cyclic oxidation—abscissa = surface concentration of S after heating for 86.4 ks (24 h) in AES system, ordinate = mass change during cyclic oxidation**

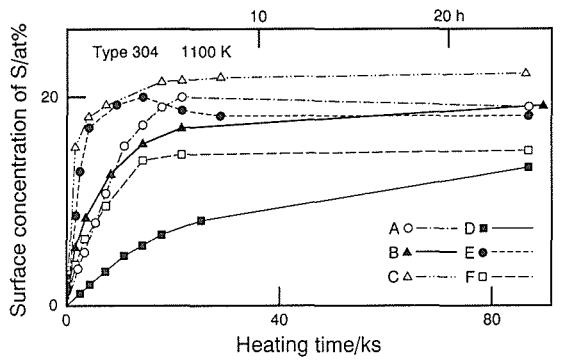


**Fig. 5 Surface segregation of S on type 304 stainless steels of different origin at 1100 K**

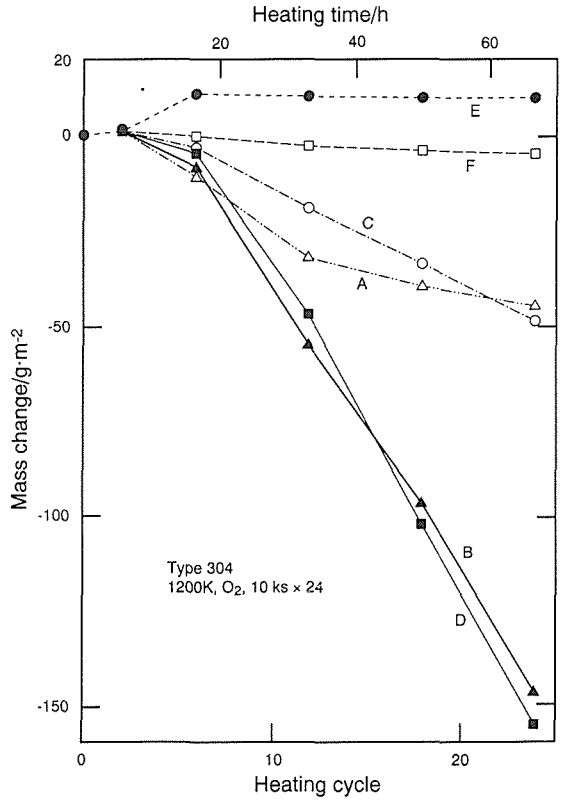


**Fig. 6 Mass change during cyclic oxidation of the same stainless steels as Fig. 5—[10 ks (2 h 47 min) in $O_2$ at 1200 K] × 24 cycles**

86.4 ks (24 h), which corresponds to the surface segregation rate of S. The ordinate indicates the mass change during cyclic oxidation. Large negative values represent extensive scale spalling. In Fig. 4 there is a clear trend that the scale spalling is progressively extensive with increasing S segregation rate. This result supports the "detrimental effect of S" model and suggests very strongly that REM suppresses the spalling by trapping S as a sulfide in alloy matrix. Afterwards numerous results in accord with ours were reported[2–7].

### 3.2 Results against the S Model

Similar experiments were made on commercial stainless steels to obtain further evidence for the detrimental effect of S. The results are given in Figs. 5 and 6. The surface segregation of S was comparably rapid except on 304-D steel (Fig. 5). But contrary to the expectation the extent of spalling scatters largely (Fig. 6). Ruthra et al.[8] also obtained results against the S model. These results show that oxidation experiment does not suffice for the elucidation of oxidation mechanism very probably because of a wide variety of oxide features as stated in Introduction. Thus in further experiments spalling charac-

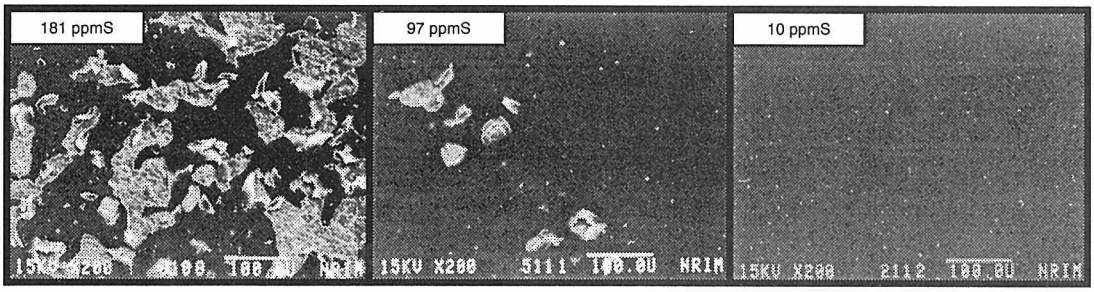


**Fig. 8 Surface feature of the same stainless steels as Fig. 7—coated with $Al_2O_3$ and heated cyclically in $O_2$ at 1100 K, [heating for 10 ks (2 h 47 min)] × 3 cycles**

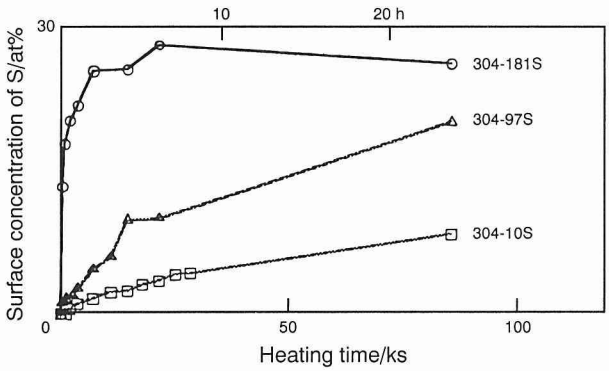


**Fig. 7 Surface segregation of S on type 304 stainless steels with different S content at 1100 K**

teristics were mainly investigated on $A1_2O_3$ coating film applied under the same conditions.

## 4. Segregation of S and Spalling of Coating Film

### 4.1 Effect of S Content[9]

The first experiment using $A1_2O_3$ coating film was made on type 304 stainless steels with different S content. The surface segregation rate of S was measured on three sorts of steels (304-10S, -97S and -181S). It increases with increasing S content (Fig. 7). Then the freshly polished samples were coated with $A1_2O_3$ and heated cyclically in a stream of $O_2$ at 1100 K. One cycle consisted of 10 ks (2 h 47 min) of heating and 2 ks (33 min) of cooling at R.T. Figure 8 shows the surface features after 3 cycles of heating. The extent of spalling increased with increasing S segregation rate. These results support very strongly the model that S promotes the spalling.

### 4.2 Effect of REM Addition[9]

The surface segregation of S was measured on type 310S stainless steels with and without REM addition (Fig. 9). The segregation is seen to be suppressed by REM. Then $Al_2O_3$ coated specimens were cyclically heated in the same manner as above. The thermal cycle caused extensive spalling on steels where the S segregation rate is rapid (310S, -0.05MM, -0.1MM) (Fig. 10). Similar experiments were made on other steels and S promoted always the spalling (Figs. 11 and 12). These results support very well the S effect model and lead to the conclusion that REM suppresses the spalling of $Al_2O_3$ film through suppressing the surface segregation of S.

Misch metal (MM) seems to be less effective in suppressing the surface segregation of S than pure La or Ce (Figs. 9 and 11). In practice, however, the apparent ineffectiveness of MM comes from relatively high S content in steels containing MM. Table 4 shows the atomic concentration of S and REM in steels used for this

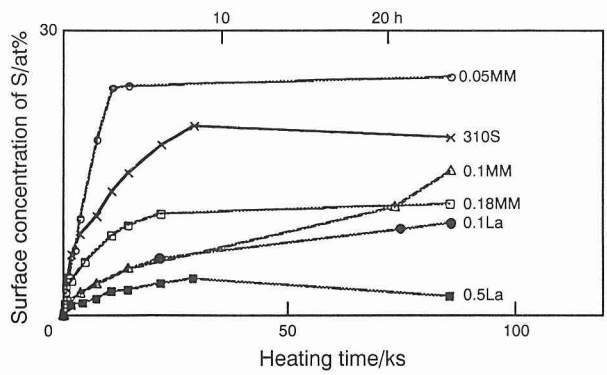


**Fig. 9 Surface segregation of S on type 310S stainless steels with and without REM addition at 1100 K**

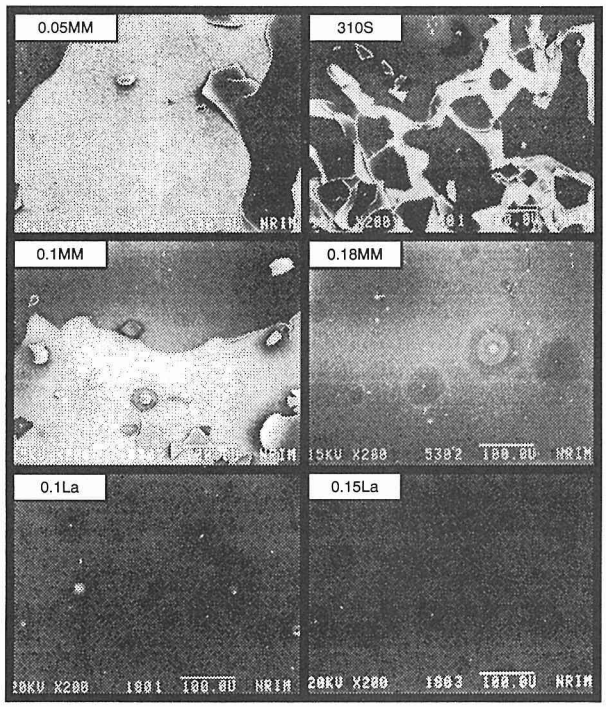


Fig. 10 Surface feature of the same stainless steels as Fig. 9—coated with $Al_2O_3$ and heated cyclically in $O_2$ at 1100 K, [heating for 10 ks (2 h 47 min)] × 3 cycles

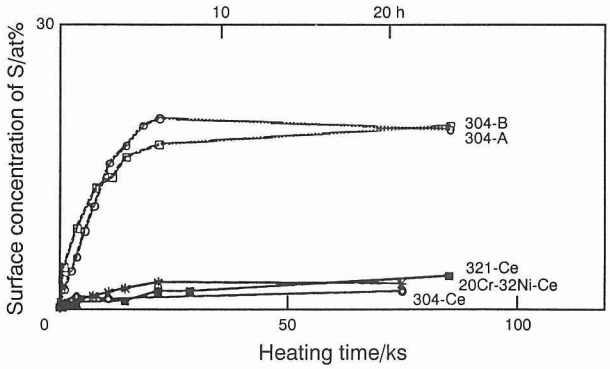


Fig. 11 Surface segregation of S on various stainless steels at 1100 K

section, and the atomic ratio [REM]/[S]. The S segregation, and accordingly the spalling, is extensive on steels with a low [REM]/[S] ratio. It means that REM can not completely trap S in them. If the S content in steels containing MM were lower, the S segregation and spalling should be well suppressed. Thus beneficial effect of REM on high temperature oxidation resistance is greatly attributed to trapping of S.

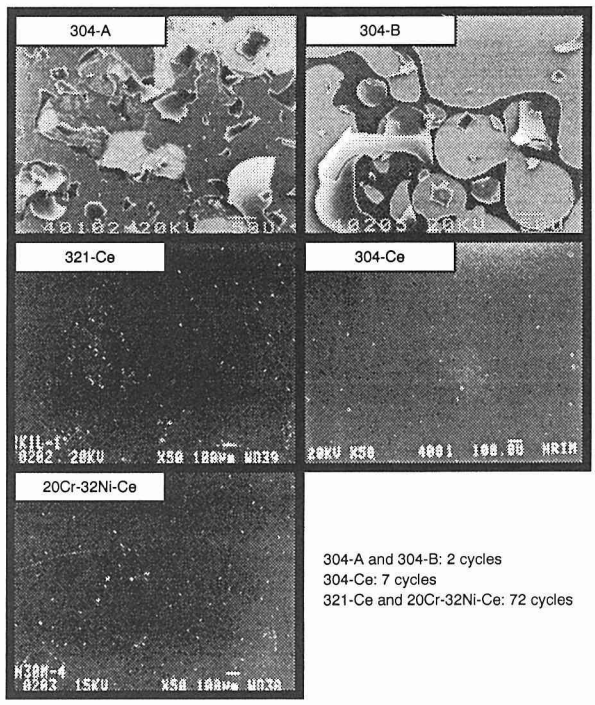


Fig. 12 Surface feature of the same stainless steels as Fig. 11—coated with $Al_2O_3$ and heated cyclically in $O_2$ at 1100 K, [heating for 10 ks (2 h 47 min)] × $n$ cycles

Table 4 [REM]/[S] ratio in REM addition steels (at%)

| Steel | S | REM | [REM]/[S] | Spalling |
|---|---|---|---|---|
| 310S-0.05MM | 0.060 | 0.019 | 0.3 | Extensive |
| 310S-0.1MM | 0.036 | 0.042 | 1.2 | Extensive |
| 310S-0.1La | 0.019 | 0.040 | 2.1 | Medium |
| 310S-0.18MM | 0.027 | 0.069 | 2.6 | Medium |
| Fe-20Cr-32Ni-Ce | 0.007 | 0.020 | 2.9 | Little |
| 321-Ce | 0.0041 | 0.013 | 3.1 | Little |
| 304-Ce | 0.0021 | 0.024 | 11.4 | Little |
| 310S-0.15La | 0.005 | 0.059 | 11.8 | Little |

### 4.3 Effect of $Y_2O_3$ Dispersion[10, 11]

Oxide dispersion strengthened (ODS) alloys are also excellent in high temperature oxidation resistance[12]. This section is devoted to systematic explanation of the excellent oxidation resistance of ODS alloys in terms of S effect. The surface segregation of S was measured in the same manner as above on commercial ODS alloys and two others (Fig. 13). The S segregation is well suppressed on ODS alloys containing more than 0.52 mass% of $Y_2O_3$. The segregation is rapid on MA957 alloy which

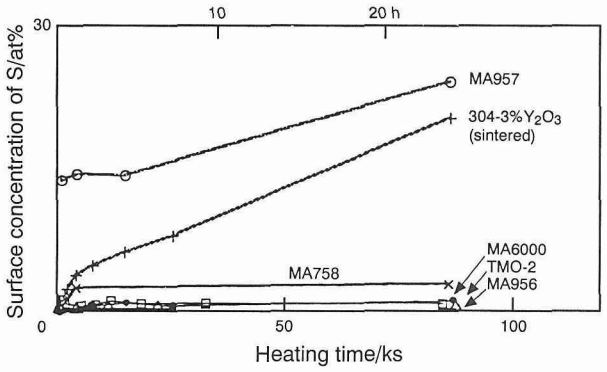


**Fig. 13 Surface segregation of S on ODS alloys at 1100 K**

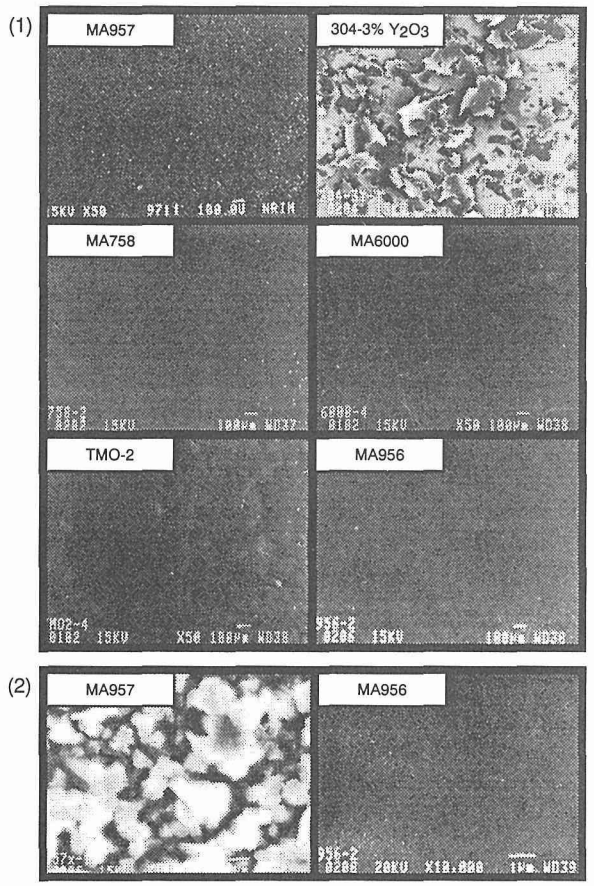


**Fig. 14 Surface feature of the same ODS alloys as Fig. 13—coated with $Al_2O_3$ and heated cyclically in $O_2$, (1) low magnification image and (2) high magnification image—MA957: 1100 K, 10 ks × 72 cycles; 304-3%$Y_2O_3$: 1200 K, 86.4 ks × 1 cycle; MA758: 1200 K, 10 ks × 12 cycles; MA6000: 1100 K, 10 ks × 72 cycles; TMO-2: 1100 K, 10 ks × 72 cycles; MA956: 1100 K, 10 ks × 72 cycles**

contains only 0.27% of $Y_2O_3$. 3% of $Y_2O_3$ can not trap S on type 304 steel which was prepared through conventional powder metallurgy, probably because dispersed oxide particles are too large and the distribution is not sufficiently uniform.

The spalling test was made in a similar manner as above (Fig. 14). In spite of much severer conditions, the spalling is well suppressed on alloys which suppress the S segregation (MA758, MA6000, TMO-2 and MA956). If $Y_2O_3$ fails to trap S, the spalling is extensive in spite of the large content of it (304-3%$Y_2O_3$). The coating film on MA957 alloy seems sound in the low magnification image (Fig. 14(1)) but the high magnification image (Fig. 14(2)) reveals that the surface is covered with oxide nodules which grew owing to the cracking of coating film. In contrast to MA957, the coating film on MA956 alloy is flat in high magnification also.

These results show that dispersed $Y_2O_3$ also suppresses the spalling and cracking through trapping S. Thus it is concluded that S promotes the spalling and cracking of $A_2O_3$ film, and that they are suppressed through suppression of the S segregation by either lowering S level in alloy or trapping S.

The spalling was not so extensive on MA957 alloy in spite of rapid S segregation rate. This fact may suggest that dispersed $Y_2O_3$ and/or mechanical alloying method provide beneficial effects other than S trapping.

### 4.4 Results on $Cr_2O_3$ Coating Film[13]

The above spalling tests were made on $Al_2O_3$ coating film. The spalling of $Cr_2O_3$ film, which is practically important in high temperature oxidation, is the subject to be discussed in this section. Figure 15 represents the surface segregation on some steels. The same type of steels were coated with $Cr_2O_3$ and cyclically heated in the same manner as above, and very similar result as $Al_2O_3$ film was obtained after 5 cycles (Fig. 16(a)). Thus the S effect model is seen to be valid in $Cr_2O_3$ film.

After 14 cycles the surface is roughened on both tested steels probably because of microcracking and subsequent oxide nodule formation (Fig. 16(b)). Although the nodule formation is more extensive on 304-97S steel than 304-10S, the difference in surface feature was not so drastic as after 5 cycles. The moderate difference is partly attributed to $Cr_2O_3$ healing layer formation at regions exposed to $O_2$ owing to spalling of coating film. The

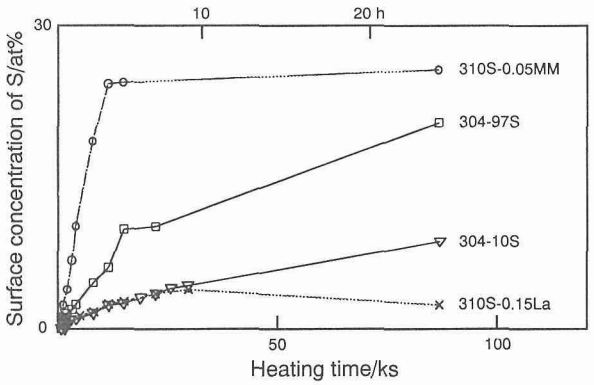


**Fig. 15 Surface concentration of S on some stainless steels at 1100 K**

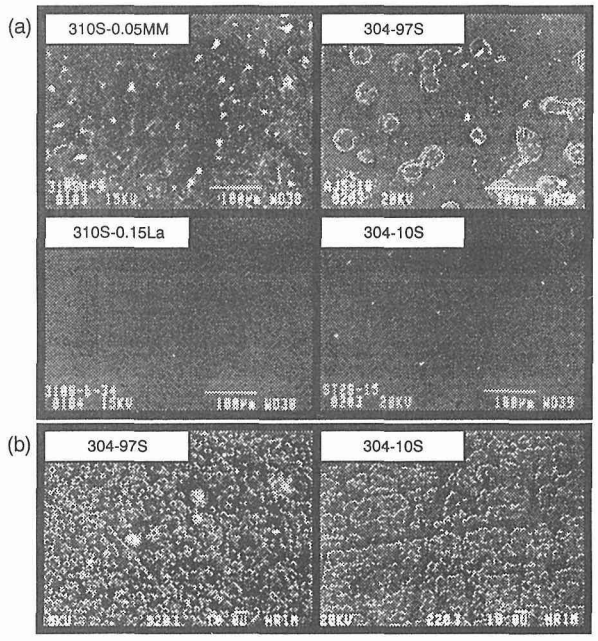


**Fig. 16 Surface feature of the same stainless steels as Fig. 15—coated with $Cr_2O_3$ and heated cyclically in $O_2$ at 1100 K, (a) 10 ks (2 h 47 min) × 5 cycles and (b) 10 ks × 14 cycles**

spalling of $Cr_2O_3$ coating film was generally less extensive than $Al_2O_3$ coating film. Thus $Cr_2O_3$ film is considered to be less sensitive to S segregation. Hou et al.[14] also reported that $Cr_2O_3$ scale has a higher tolerance for S than $Al_2O_3$.

### 4.5 Interfacial Segregation of S[9]

The above discussion was made on the basis of surface segregation but not interfacial segregation. The

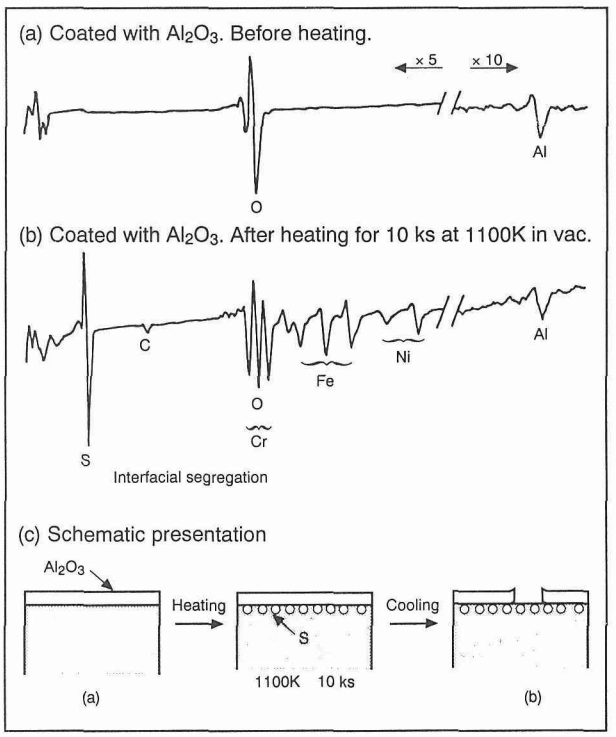


**Fig. 17 AES spectrum on type 310S-0.05MM steel coated with $Al_2O_3$**

spalling should be promoted by S segregated at oxide film/alloy interface. The next experiment was made to detect interfacial segregation of S. For this purpose type 310S-0.05MM steel, on which surface segregation of S is very rapid (Fig. 9), was coated with $Al_2O_3$ in the same manner as above and heated at 1100 K for 10 ks (2 h 47 min) in the AES system. The AES spectra are given in Fig. 17. Before heating only Al and O were observed (Fig. 17(a)). No spalling was observed at high temperature but the spalling took place during cooling in a similar manner as in $O_2$. The AES spectrum after heating is given in Fig. 17(b) where a large S peak is observed. This result shows that S segregates at $Al_2O_3$/steel interface as well as free surface. This interfacial S is considered to promote the spalling, as schematically drawn in Fig.17(c).

### 4.6 Bond Weakening by Interfacial S[15]

The above results indicate that S promotes the spalling, but it is not clear how S does so. Thus the alteration in chemical bonding at $Al_2O_3$/alloy interface was investigated by means of X-ray photoelectron spectroscopy (XPS). $Al_2O_3$ was deposited on three sorts of alloys in a

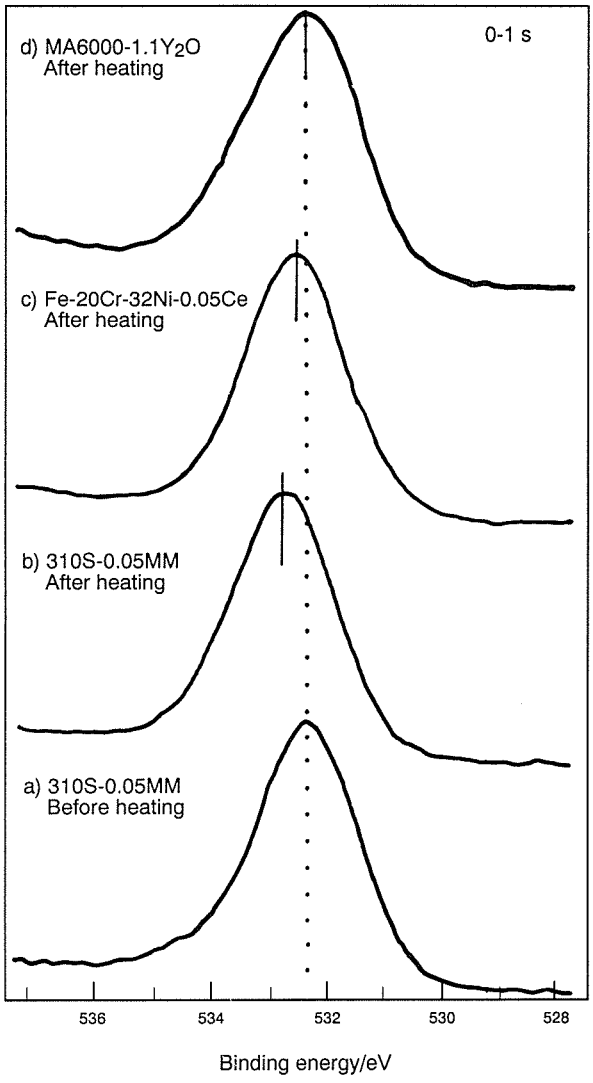


**Fig. 18 XPS spectra of O-1 s on some alloys coated with an $Al_2O_3$ film thinner than one monolayer and heated for 3.6 ks (1 h) at 1100 K in the XPS system**

thickness less than one monolayer in an XPS apparatus and heated at 1100 K for 3.6 ks (1 h). XPS spectrum of O-1 s, was taken before and after the heating. A spectrum on type 310S-0.05MM steel before heating is shown in Fig. 18(a) and that after heating in Fig. 18(b). A clear peak shift is observed between them.

There exists some chemical bonding between deposited $Al_2O_3$ and substrate alloy. The peak before heating (Fig. 18(a)) indicates the binding energy of O-1 s electron in $Al_2O_3$, and refers to the bonding between the steel and $Al_2O_3$ as deposited. The interfacial segregation of S by heating alters the steel- $Al_2O_3$ bonding, and hence the binding energy of O-1 s electron. The observed peak shift corresponds to this alteration in the binding energy (Fig. 18(a, b)). Although alteration in binding energy does not afford direct information as to whether the steel-$Al_2O_3$ bond is weakened or strengthened, the above alteration is reasonably considered to be in the bond weakening direction, for the spalling is very extensive on this steel.

In contrast to 310S-0.05MM steel the peak shift is very small on Fe-20Cr-32Ni-0.05Ce alloy and negligible on MA6000 alloy (Fig. 18(c), (d)). Hence it is considered that the alteration in chemical bonding, accordingly the bond weakening, does not occur on these two alloys where the S segregation is well suppressed. In fact the spalling is also well suppressed on them (Figs. 12 and 14). Ruthra et al. claimed that Y segregates to oxide/alloy interface to strengthen the bond between them which is basically weak[8]. The above result, however, indicates that S weakens the bond which is basically strong.

### 4.7 S Trapping by $Y_2O_3$[11]

It is reasonable that REMs suppress the surface segregation of S through trapping it as a stable sulfide within the alloy matrix, because REMs are very active elements. But it is unlikely that $Y_2O_3$, which is a very stable oxide, turns into a sulfide or oxysulfide to trap S. The standard free energy of formation of oxide (absolute value $|\Delta G^\circ_{ox}|$) is generally greater than that of the corresponding sulfide ($|\Delta G^\circ_{sul}|$).

Apart from sulfide formation, the interfacial energy between particles and matrix increases with decreasing particle radius. It is possible that the dispersed $Y_2O_3$ particles, which have a very small radius (generally several tens of nm), adsorb S in virtue of the high interfacial energy. Thus the trapping of S by dispersed $Y_2O_3$ was examined by means of analytical electron microscope. Figure 19 shows a transmission electron microscope (TEM) image of dispersed $Y_2O_3$ particle in MA956 alloy. Spot analysis was made on some of these particles and alloy matrix regions with energy dispersive X-ray microanalyzer (EDX) attached to the TEM. The results are given in Table 5 which shows that S concentration in the particle regions is one or two orders of magnitude greater than the value by chemical analysis. Thus it is concluded that S is trapped by $Y_2O_3$ particles,

Fig. 19 TEM image of MA956 alloy

Table 5 Local concentration in MA956 alloy measured with analytical electron microscope (mass%)*

| | S | Y | Cr | Al |
|---|---|---|---|---|
| Particle region 1 | 0.31 | 6.80 | 16.62 | 8.01 |
| Particle region 2 | 0.13 | 6.90 | 16.79 | 9.44 |
| Matrix region 1 | 0.00 | 0.01 | 19.86 | 5.60 |
| Matrix region 2 | 0.00 | 0.42 | 20.85 | 4.58 |
| Chemical analysis | 0.004 | | 19.76 | 4.60 |

* Oxygen can not be analyzed with this apparatus.

and that the S trapping is one of important characteristics of $Y_2O_3$.

### 4.8 Reexamination of Commercial 304 Steels[9]

The above results of $Al_2O_3$ coating film clearly show the detrimental effect of S and beneficial effect of REM and $Y_2O_3$. Although the S effect was not always reflected in spalling characteristics of oxide scale (Fig. 5 and 6), the spalling of coating film is expected to be promoted by S even on the same steels as Fig. 6. Thus these steels

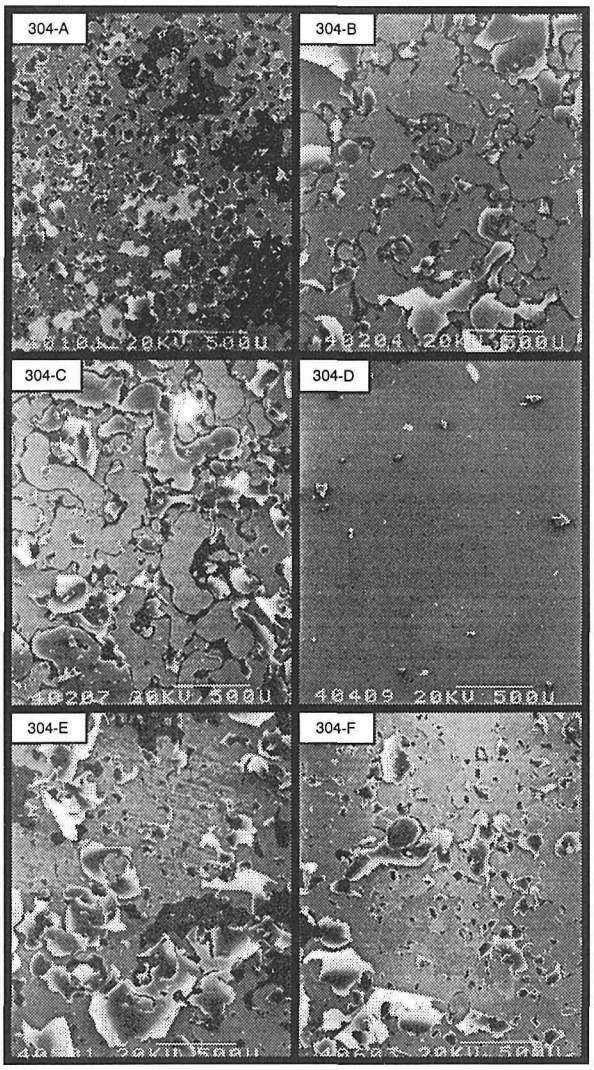


Fig. 20 Surface feature of the same type steels as Figs. 5 and 6—coated with $Al_2O_3$ and heated cyclically in $O_2$ at 1100 K, [heating for 10 ks (2 h 47 mm)] × 2 cycles

were coated with $Al_2O_3$ and heated cyclically in the same manner as above. The surface features after 2 cycles are given in Fig. 20 which shows extensive spalling reflecting the rapid S segregation rate. In addition the spalling is slight on type 304-D steel in accord with the moderate S segregation rate (Fig. 5). The detrimental effect of S is reconfirmed in this result.

## 5. Factors other than S Effect

Three factors examined in this research are schematized in Fig. 21.

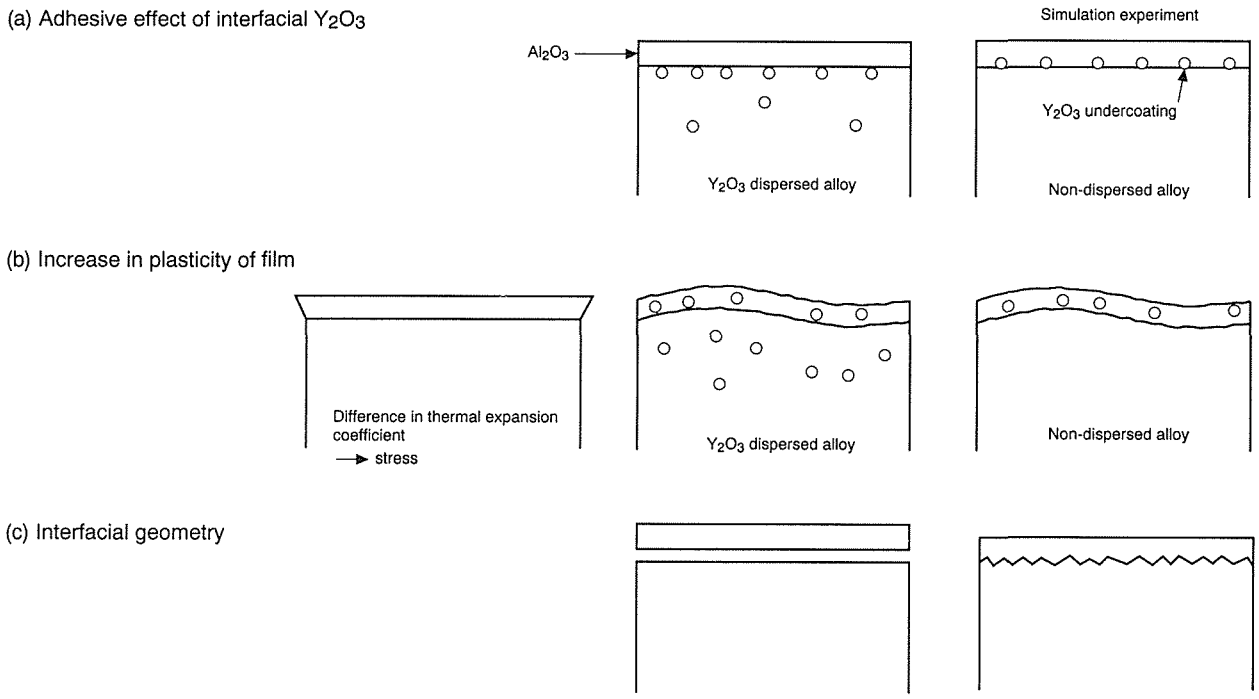


**Fig. 21 Schematic presentation of factors possibly influencing the spalling characteristics**

### 5.1 Adhesive Effect of $Y_2O_3$[11]

During the AES measurement Y or $Y_2O_3$ was found to be enriched at the surface of ODS alloys. Figure 22 shows an AES spectrum taken on TMO-2 alloy with enlarged low energy regions. Heating at 1100 K produced several peaks which can be assigned to Y[16]. A peak of Y at 127eV is considered to be largely deformed by a peak of P. The Y-enriched layer was expected to act as an adhesive of $Al_2O_3$ film to substrate alloy in analogy with TiC surface precipitation which had been found to have an adhesive effect[17, 18].

The adhesive effect of Y was examined by simulation experiment using $Y_2O_3$ undercoating on dispersion-free alloys (Fig. 21(a)), because experiments using ODS alloys can not distinguish the adhesive effect from the S trapping effect. A very thin $Y_2O_3$ undercoating layer was deposited on some alloys and then overcoated with $Al_2O_3$ in the same manner as above.

At first the undercoating condition was determined. Figure 23 shows AES spectra on $Y_2O_3$ coated surface. Fe peaks from the substrate are large after 23 s of coating, but very small after 120 s. Considering large Ni peaks on TMO-2 alloys (Fig. 22), the undercoating was made for 120 s or less.

Samples coated with $Al_2O_3$ with and without undercoating were heated cyclically in a similar manner as above. The surface features are presented in Fig. 24. Contrary to the expectation, the undercoating did not have any effect except 600 s. Regardless of undercoating the spalling is extensive on alloys having a large S segregation rate (304-181S, 304-$Y_2O_3$), and suppressed on alloys having a small rate (304-10S, MA956). Thus it is seen that the suppression of S segregation by $Y_2O_3$ is much more important than the adhesive effect.

Although 600 s of undercoating on 304-181S steel suppressed the spalling to some extent, this layer is too thick to simulate a Y-enriched layer on ODS alloys. This result, however, will provide a useful suggestion in development of ceramic coating technique.

### 5.2 Increase in Film Plasticity[11]

Some researchers reported that the plasticity of $Al_2O_3$ scale increased with incorporation of Y in it[19]. The increased plasticity should suppress the spalling. The plasticity effect was examined by a simulation experiment using $Al_2O_3$ coating film doped with $Y_2O_3$ (Fig. 21(b)). A small piece of $Y_2O_3$, 3 × 3 × 1 or 10 × 10 × 1 mm, was

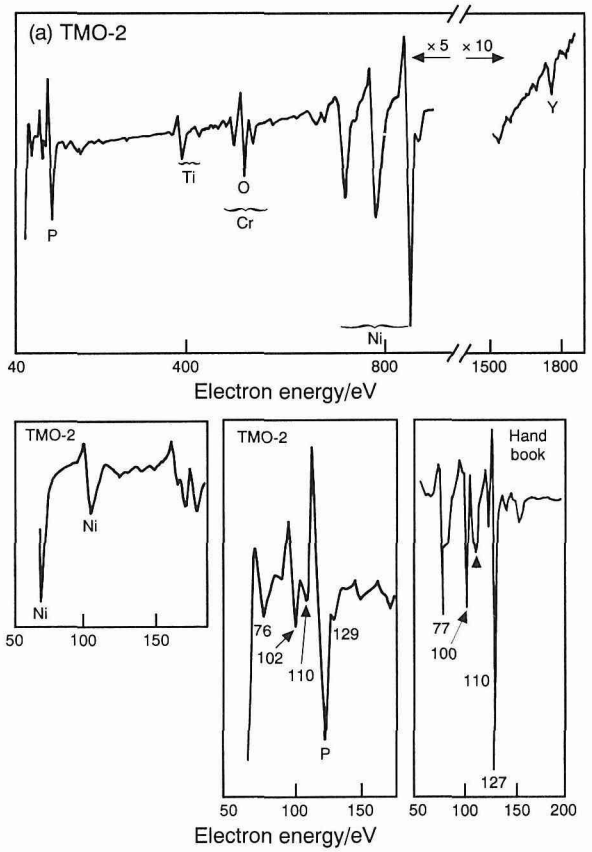


Fig. 22 AES spectrum on an ODS alloy TMO-2—upper: after heating for 86.4 ks (24 h) at 1100 K, under: (left) low energy region before heating, (center) low energy region after heating, and (right) spectrum of Y[16]

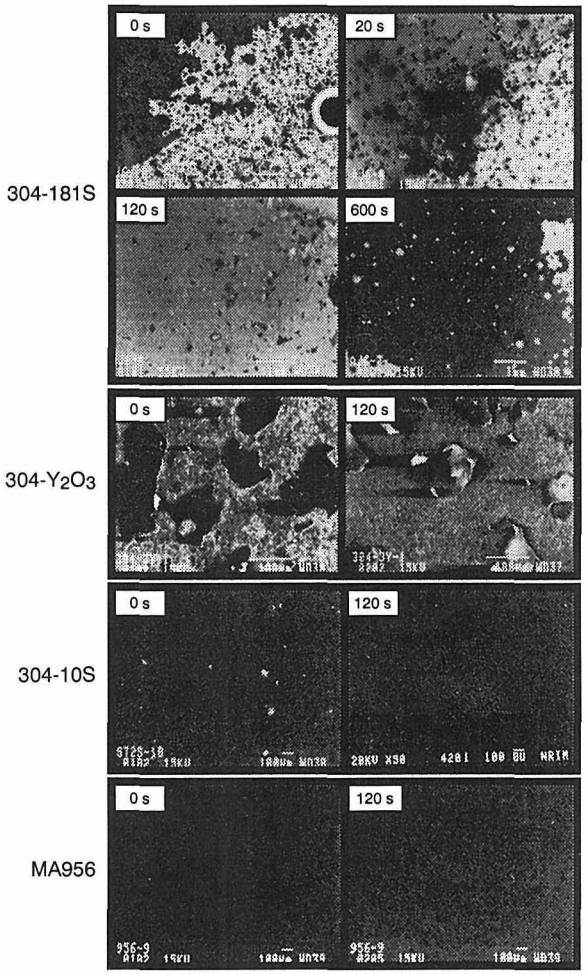


Fig. 24 Surface feature of $Al_2O_3$ coated alloys with and without $Y_2O_3$ undercoating and cyclically heated in $O_2$—undercoating time is shown at the top left corner of each photograph. Type 304-181S: 1100 K, 10 ks (2 h 47 min) × 14 cycles; Type 304-$Y_2O_3$: 1200 K, 86.4 ks (24 h) × 1 cycle; Type 304-10S: 1100 K, 10 ks × 36 cycles; MA956: 1200 K, 10 ks × 12 cycles

placed on the $Al_2O_3$ target of 50 mm ϕ in diameter, and the two materials were simultaneously sputtered onto stainless steel samples having a different S segregation rate. Then the samples were cyclically heated at 1100 K

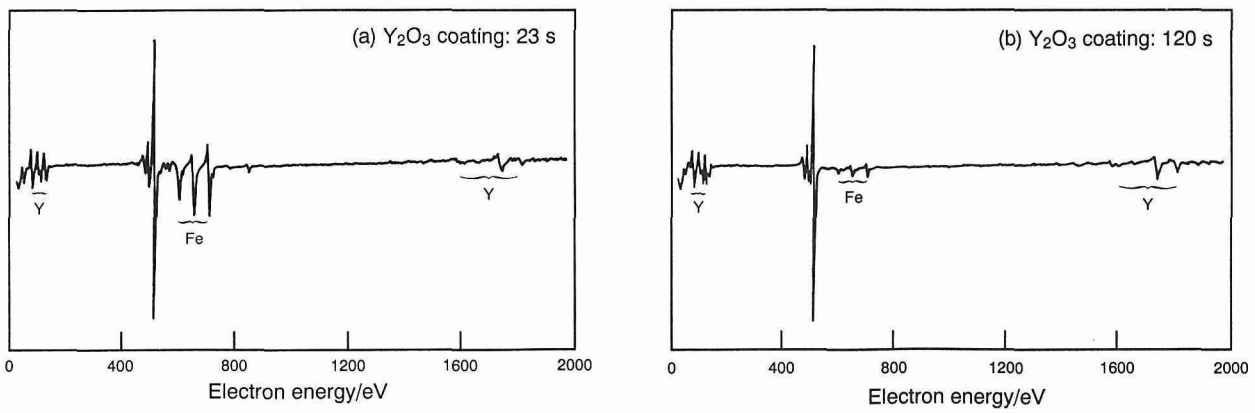


Fig. 23 AES spectra on type 304 steel coated with $Y_2O_3$

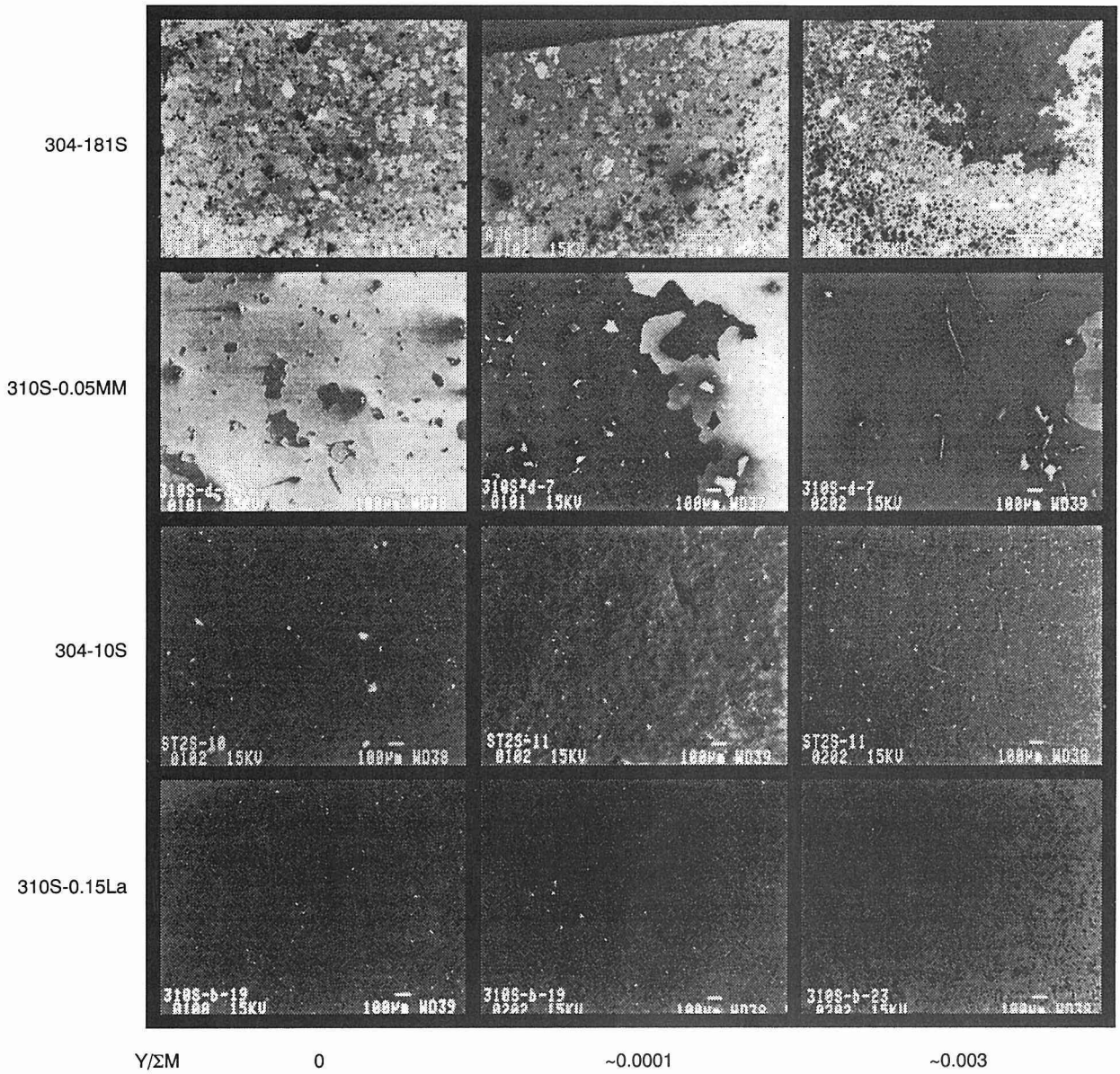


**Fig. 25 Effect of $Y_2O_3$ doping into $Al_2O_3$ coating film on the spalling characteristics in thermal cycling in $O_2$ at 1100 K—left: without $Y_2O_3$; center: coated with $Al_2O_3$-$Y_2O_3$, a $Y_2O_3$ piece of 3 × 3 × 1 mm was placed on $Y_2O_3$ target; right: coated with $Al_2O_3$-$Y_2O_3$, a $Y_2O_3$ piece of 10 × 10 × 1 mm was placed on $Y_2O_3$ target. Type 304-181S: 10 ks (2 h 47 min) × 14 cycles; Type 310S-0.05MM: 10 ks × 3 cycles; Type 304-10S: 10 ks × 36 cycles; Type 310S-0.15La: 10 ks × 20 cycles; Y/ΣM: Atomic ratio of Y to total metallic elements in $Al_2O_3$ coating film**

in the same manner as above. Figure 25 shows the surface features after thermal cycling. The $Y_2O_3$ doping had some effect in lightening the spalling on 310S-0.05MM steel up to 3 cycles, but practically no effect on 310-181S steel after 14 cycles. In contrast to them the spalling was suppressed even after 20 or 36 cycles on steels having a small S segregation rate regardless of $Y_2O_3$ doping. This result confirms again the importance of the S effect (304-10S, 310S-0.15La).

### 5.3 Effect of Interfacial Geometry[20]

Above spalling tests were always made on smooth surface polished with diamond slurry. It is plausible that an $Al_2O_3$ film is more resistant to the spalling on roughened surface than smooth one (Fig. 21(c)). Type 310S-0.05MM steel samples having a large S segregation rate were ground with different emery papers, or polished with diamond slurry for comparison. Then they were

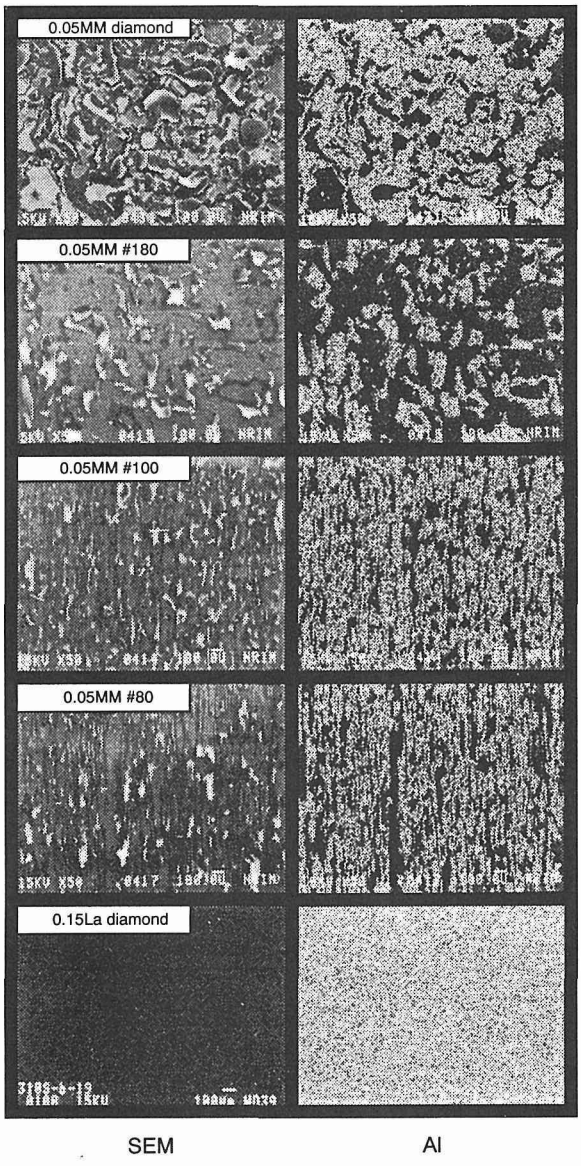


**Fig. 26 SEM and characteristic X-ray images of Al on type 310S steels with different surface roughness (ground with different emery paper or polished with diamond slurry)—coated with $Al_2O_3$ and heated cyclically in $O_2$ at 1100 K. Type 310S-0.05MM: 10 ks (2 h 47 min) × 2 cycles; Type 310S-0.15La: 10 ks × 20 cycles**

coated with $Al_2O_3$ and heated cyclically at 1100 K in the same manner as above. Figure 26 shows SEM images and characteristic X-ray images of Al on the tested samples. The spalling was extensive on the smooth surface polished with diamond slurry, and any beneficial effect was not observed on the surface ground with emery paper #180. Grinding with emery #100 and 80 lightened the spalling very slightly up to 2 cycles, although it has no

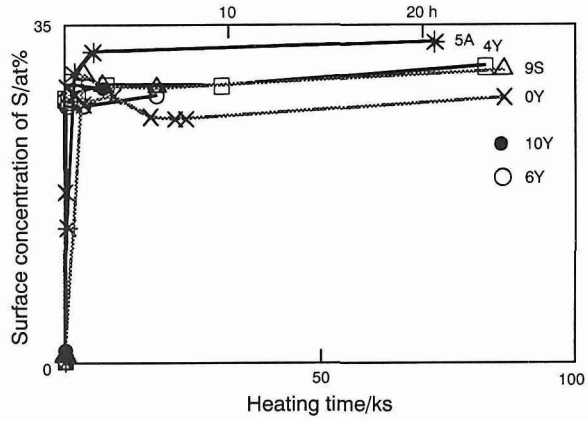


**Fig. 27 Surface segregation of S on Fe-20Cr alloys with various oxide dispersion at 1100 K**

practical importance. By contrast, the spalling was well suppressed on a smooth surface of 310S-0.15La steel having a small S segregation rate. These results show that the bond weakening by S has much more substantial importance than the interfacial geometry effect.

## 6. Further Study on ODS Alloys with Various Oxide

Current ODS superalloys are prepared by mechanical alloying method and contain $Y_2O_3$ as dispersoid. In this section a comparison is made between dispersion of $Y_2O_3$ and other oxides.

### 6.1 Ferritic Alloys[20, 25]

Fe-20Cr alloys with and without oxide dispersion were prepared by mechanical alloying method. The dispersoid is $Y_2O_3$, $Al_2O_3$, $SiO_2$, $ZrO_2$ or $Y_2O_3$ + $Al_2O_3$. The chemical composition is given in Table 2.

Figure 27 shows the surface segregation rate of S at 1100 K. Contrary to the expectation, the S segregation was very rapid on any alloys. The oxide particles may be insufficiently fine and dispersed nonuniformly, and accordingly even $Y_2O_3$ is considered to be unable to trap S. The spalling test was made in a similar manner as above up to 72 cycles, and the surface features are represented in Fig. 28. Contrary to the expectation once again, the spalling of $Al_2O_3$ film was negligible on any alloys in spite of the rapid S segregation, although there were numerous little oxide nodules. The masking of S effect can be attributed to difference in thermal expansion coefficient which is smaller between $Al_2O_3$ and ferritic

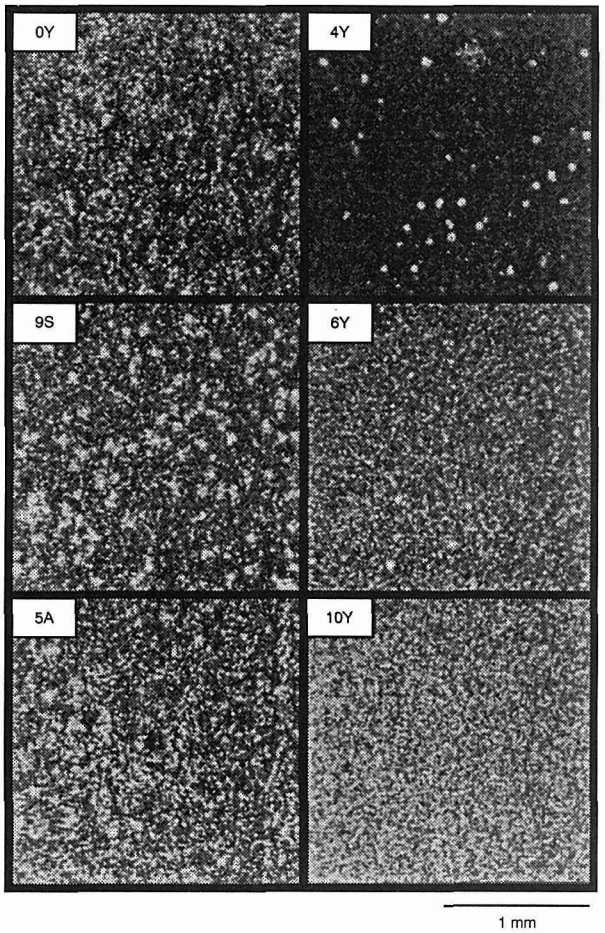


Fig. 28 Surface feature of the same alloys as Fig. 27—coated with $Al_2O_3$ and heated cyclically in $O_2$ at 1100 K, [heating for 10 ks (2 h 47 min)] × 72 cycles

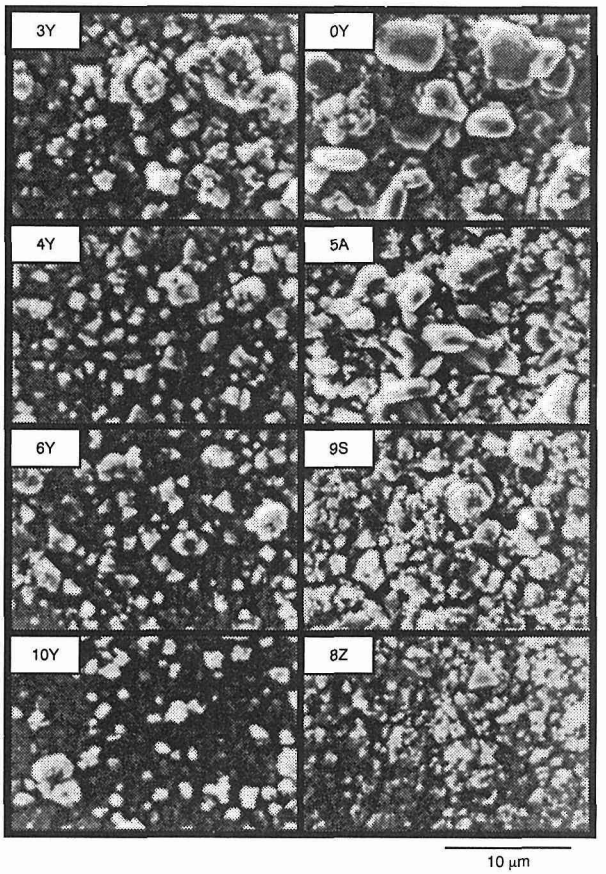


Fig. 29 Surface feature of Fe-20Cr alloys with various oxide dispersion oxidized cyclically in $O_2$ at 1100 K, [oxidation for 10 ks (2 h 47 min)] × 72 cycles

Table 6 Thermal expansion coefficients at 1100 K

| | |
|---|---|
| $Al_2O_3$[21] | 7~9 × $10^{-6}$ |
| Ferritic stainless steel[22] | 11~12 |
| Austenitic stainless steel[22] | 19~20 |
| MA956[23] | 14 |
| MA6000[24] | 16 |

alloys than austenitic alloys (Table 6). Smaller difference leads to smaller stress and accordingly to smaller extent of spalling.

Cyclic oxidation test was also made on these alloys at 1100 K[25]. Figure 29 represents surface features after 72 cycles. Numerous oxide nodules show frequent cracking of oxide scale, but nodules are less extensive on alloys with higher $Y_2O_3$ content. This aspect is indicated more quantitatively in Fig. 30. The reflectance of oxidized sample surface increases with increasing $Y_2O_3$ content. The reflectance on the ordinate is expressed as a ratio of intensity of reflected light after oxidation to before. Figures 27, 29 and 30 show that dispersed $Y_2O_3$ suppresses the scale cracking to some extent in spite of S segregation. Thus $Y_2O_3$ is considered to have an effect other than S trapping in suppressing spalling and cracking, although this effect is not so drastic as S trapping. This additional effect is considered to act only in growing oxide scale, because $Y_2O_3$ has little effect for $Al_2O_3$ coating film (Fig. 28). It may be responsible for the difference in surface feature between coating film (Fig. 28) and oxide scale (Fig. 29) that $Y_2O_3$ dispersion changes scale growth mechanism from cation diffusion control to anion[26].

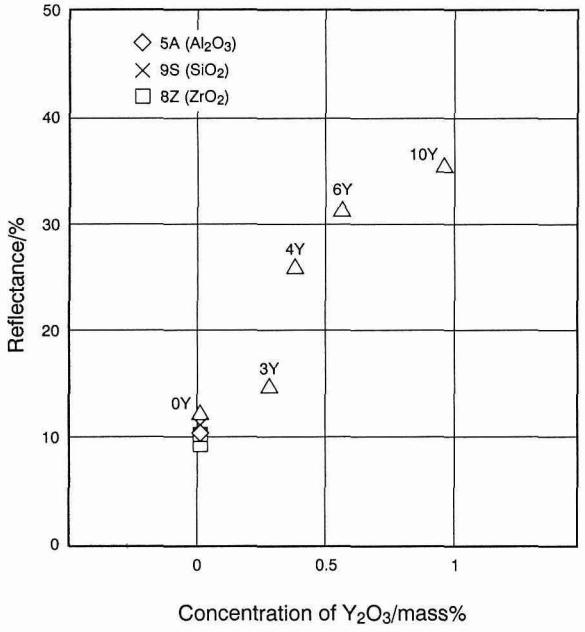


**Fig. 30 Reflectance of the surfaces shown in Fig. 29**

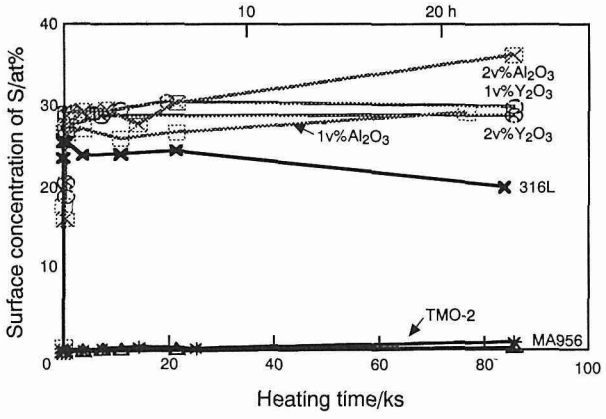


**Fig. 31 Surface segregation of S on various ODS alloys at 1100 K**

## 6.2 Austenitic Steels[20]

The result in the previous section suggests that the S trapping effect of $Y_2O_3$ appears more clearly in austenitic alloys than ferritic because of larger difference in thermal expansion coefficient in $Al_2O_3$/austenitic system. The S segregation was measured on mechanically alloyed 316 stainless steels with $Y_2O_3$ or $Al_2O_3$ dispersion, current 316L steel and reference ODS alloys. Contrary to the expectation, the S segregation was rapid on any 316 steels (Fig. 31). Then the spalling test was made in a similar manner as above (Fig. 32). In accord with the

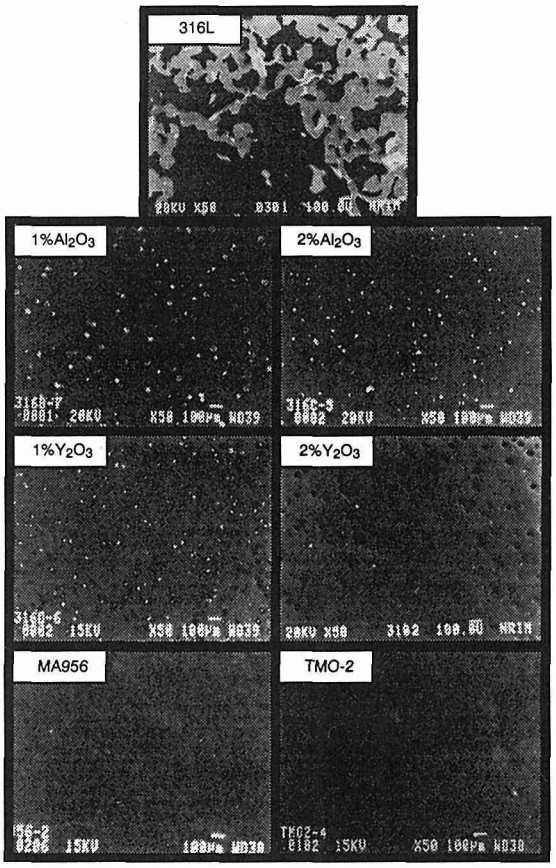


**Fig. 32 Surface feature of the same alloys as Fig. 31—coated with $Al_2O_3$ and heated cyclically in $O_2$ at 1100 K, [heating for 10 ks (2 h 47 min)] × *n* cycles. Type 316L: 1 cycle; Type 316-1%$Al_2O_3$ and 1%$Y_2O_3$: 18 cycles; Type 316-2%$Al_2O_3$ and 2%$Y_2O_3$: 12 cycles; TMO-2 and MA956: 72 cycles**

result in Section 4, the spalling of $Al_2O_3$ coating film was very extensive on type 316L steel having a high S segregation rate. Numerous cracks of $Al_2O_3$ film are observed on mechanically alloyed 316 steels, which have a high S segregation rate in spite of $Y_2O_3$ or $Al_2O_3$ dispersion, after 12 or 18 cycles, and no crack on reference ODS alloys, which have a very low S segregation rate, after 72 cycles. Although this result supports the S effect model, it is suggested that there is a mechanism other than cited above, because the spalling was more extensive on the cast 316L steel than mechanically alloyed steels. Since there is little difference in the cracking and spalling characteristics between $Y_2O_3$ dispersion and $Al_2O_3$, the difference between the cast steel and mechanically alloyed ones can be attributed to the method

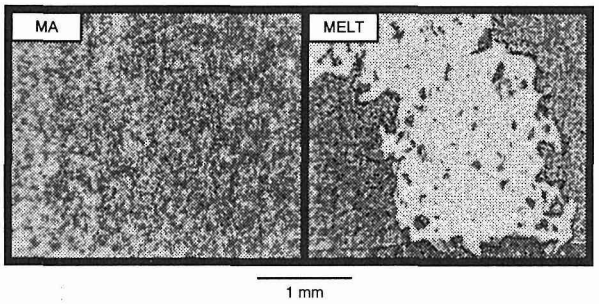


**Fig. 33 Surface feature of Fe-20Cr alloys coated with $Al_2O_3$ and heated cyclically in $O_2$ at 1100 K, [heating for 10 ks (2 h 47 min)] × *n* cycles. MA: Mechanically alloyed, 72 cycles; Melt: Mechanically alloyed and then arc-melted, 34 cycles**

of preparation. Namely mechanically alloyed steels may be more resistant to the spalling than cast steels.

## 7. Comparison of Mechanical Alloying with Casting[20]

The mechanically alloyed Fe-20Cr without dispersion was arc-melted. From the ingot spalling test samples were prepared in a similar manner as above. Two sorts of Fe-20Cr alloys, original and arc-melted, were coated with $Al_2O_3$ and cyclically heated. Figure 33 shows the surface feature after thermal cycling. In accord with the expectation in Section 6.2, the spalling took place on the arc-melted alloy but not on the original one. This result shows that one of desirable characteristics conferred by mechanical alloying was lost through arc-melting. A similar result is reported on an alloy prepared by current powder metallurgy and that through further melting[12].

## 8. $Y_2O_3$ Dispersed Layer by Thermal Spray Coating

Mechanical alloying, an excellent process for the preparation of high temperature alloys, is unfortunately expensive. Thus it was tried to coat cast steels with a $Y_2O_3$ dispersed layer by spray coating method. Base materials are type 304 steels with different S content and coating material is 304 steel powder implanted with $Y_2O_3$ particle. This coating material was prepared by Nara Machinery Co., Ltd.

Cyclic oxidation test was made on spray coated and non-coated samples. Mass loss is large on high S steels without spray coating but remarkably suppressed on spray coated steels (Fig. 34). It is small on low S steel regardless of spray coating. This result indicates that the $Y_2O_3$ dispersed layer by spray coating is also effective in suppressing the spalling of oxide scale.

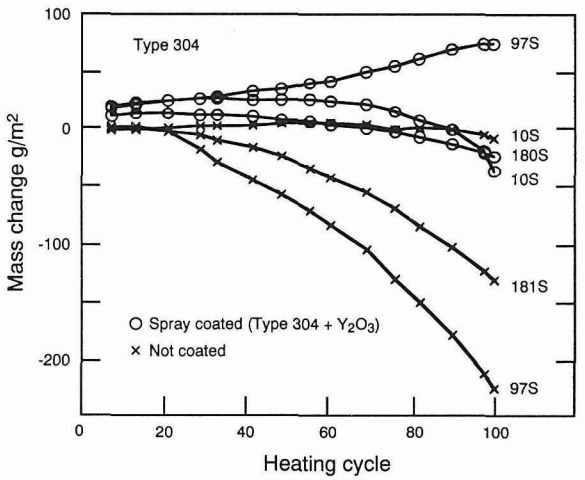


**Fig. 34 Mass change during cyclic oxidation of type 304 steels with different S content in $O_2$ at 1100 K—10 ks (2 h 47 min) × 100 cycles**

## 9. Diffusion of Alloying Elements into $Al_2O_3$ Coating Film[11, 27]

Oxide scales grow by cationic or anionic diffusion in them if gas penetration is negligible. Thus many researchers have made great effort to elucidate the diffusion mechanism in oxides. This chapter is devoted to the effect of dispersed $Y_2O_3$ on the diffusion of alloying elements into $Al_2O_3$ coating film.

### 9.1 Existing ODS Alloys

Some ODS alloys and reference alloys were coated with $Al_2O_3$ and heated continuously in $O_2$ for 86.4 ks (24 h) at 1200 K. Concentration profiles were taken on cross-sections of diffusion-annealed samples (Fig. 35). Diffusion of Mn, Cr and Ti is rapid on type 321 and 310S-0.15La steels. La suppresses the surface segregation of S but does not the diffusion. In contrast with dispersion-free steels, the diffusion is well suppressed on ODS alloys except MA957 alloy. The $Y_2O_3$ content in MA957 is considered too small to suppress the diffusion. In any way the diffusion suppression is considered to be one of characteristics of suitably dispersed $Y_2O_3$. In the following sections two mechanisms are examined for the diffusion suppression effect of $Y_2O_3$.

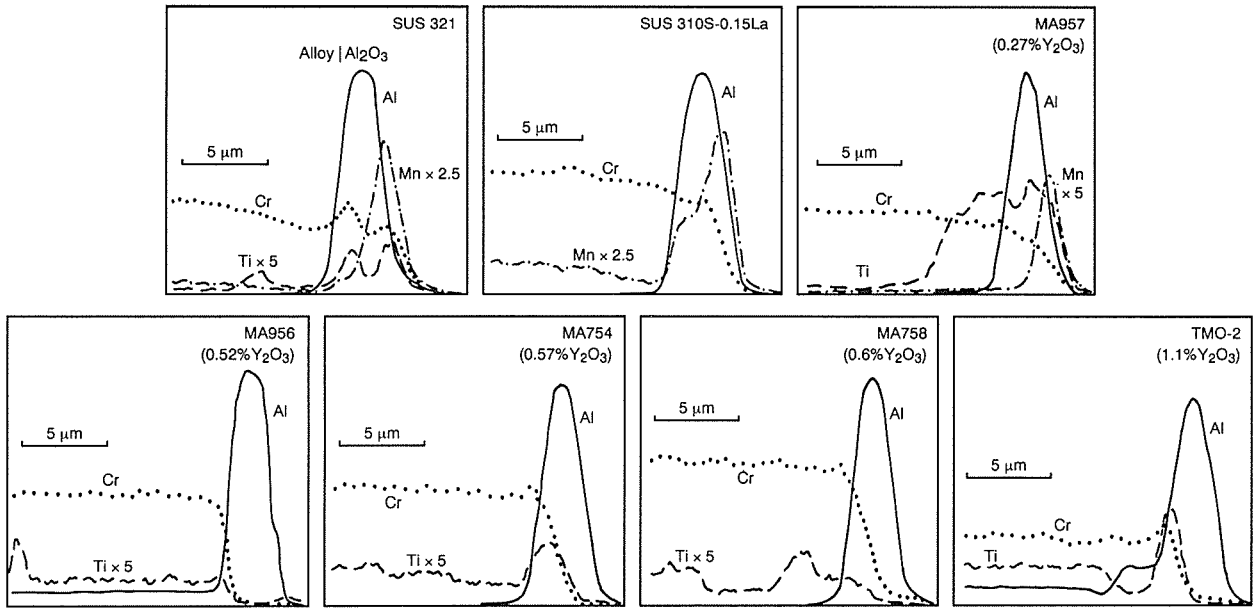


**Fig. 35 Diffusion of alloying elements into $Al_2O_3$ coating film on some alloys—diffusion-annealed in $O_2$ at 1200 K for 86.4 ks (24 h)**

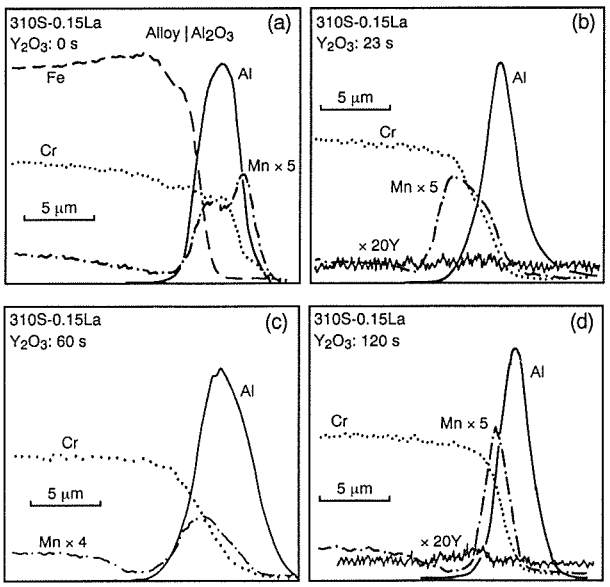


**Fig. 36 Diffusion of alloying elements into $Al_2O_3$ coating film with and without $Y_2O_3$ undercoating—diffusion-annealed in $O_2$ at 1200 K for 86.4 ks (24 h)—undercoating time: (a) 0 s, (b) 23 s, (c) 60 s, and (d) 120 s**

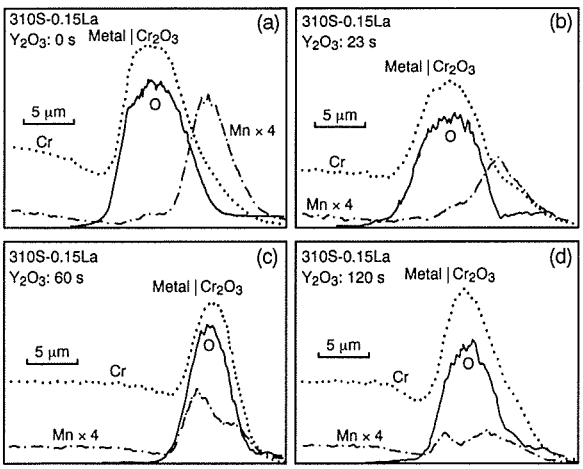


**Fig. 37 Diffusion of alloying elements into $Cr_2O_3$ coating film with and without $Y_2O_3$ undercoating—diffusion-annealed in $O_2$ at 1200 K for 86.4 ks (24 h)—undercoating time: (a) 0 s, (b) 23 s, (c) 60 s, and (d) 120 s**

## 9.2 Diffusion Barrier

As stated in Section 5.1, Y was enriched at the surface of ODS alloys at 1100 K (Fig. 22). Thus the Y-enriched layer was expected to act as a diffusion barrier. The result in Fig. 35 supports the expectation but can not distinguish the diffusion barrier formation effect from possible other effects. To examine the barrier formation effect a simulation experiment was made using $Y_2O_3$ undercoating in a similar manner as the adhesive effect experiment (Section 5.1).

The substrate alloy is type 310S-0.15La steel, which suppresses the surface segregation of S. The S segregation might suppress the diffusion by cutting the bond,

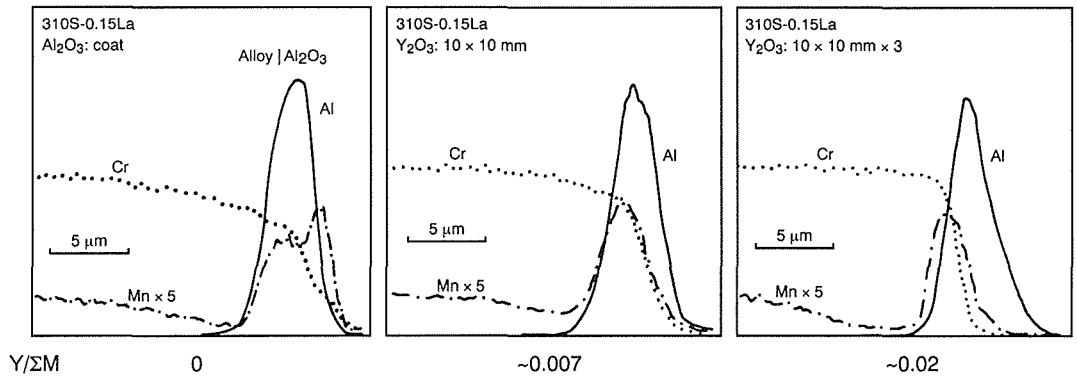


**Fig. 38 Diffusion of alloying elements into $Al_2O_3$ coating film with and without $Y_2O_3$ doping—diffusion-annealed in $O_2$ at 1200 K for 86.4 ks (24 h)—left: without doping; center: 1 piece of $Y_2O_3$ (10 × 10 × 1 mm) was placed on the $Al_2O_3$ target; right: 3 pieces of $Y_2O_3$ were placed—Y/ΣM: atomic ratio of Y to total metallic elements in $Al_2O_3$ coating film**

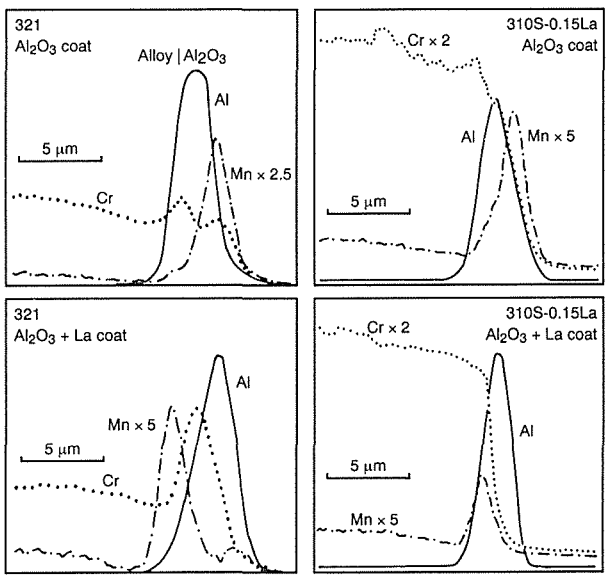


**Fig. 39 Diffusion of alloying elements into $Al_2O_3$ coating film with and without La doping—diffusion-annealed in $O_2$ at 1200 K for 86.4 ks (24 h)**

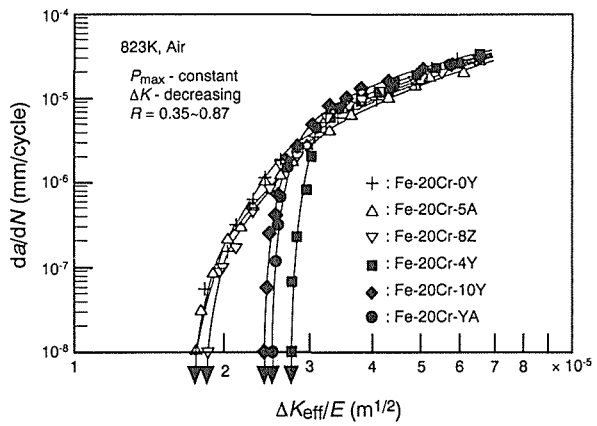


**Fig. 40 Fatigue crack propagation rate of Fe-20Cr alloys with and without oxide dispersion at 823 K in air—*a*: crack length, *N*: number of cycles, $\Delta K_{eff}$: effective stress intensity amplitude, *E*: Young's modulus, *P*: load, and *R*: load ratio ($P_{min}/P_{max}$)**

namely forming an interstice, between $Al_2O_3$ film and substrate alloy. This steel was undercoated with $Y_2O_3$, coated with $Al_2O_3$ and diffusion-annealed in $O_2$ for 86.4 ks (24 h) at 1200 K. The concentration profile on the cross-section is given in Fig. 36, which indicates the diffusion suppression by the undercoating and accordingly supports the diffusion barrier model. Thus the diffusion-barrier formation is considered to be one of desirable characteristics of ODS alloys.

A similar experiment was made for $Y_2O_3$ undercoating-$Cr_2O_3$ coating systems (Fig. 37). The diffusion of Mn is very rapid without undercoating, but moderately suppressed by the undercoating. Thus the diffusion barrier model is applicable to $Cr_2O_3$ film also, although more poorly than $Al_2O_3$ film.

## 9.3 Incorporation of $Y_2O_3$ and REM into $Al_2O_3$ Film

Many researchers accept that the diffusion mechanism in oxide scale is modified by reactive elements incorporation[28]. Since such elements are, although incorporated into oxide scale during oxidation, not incorporated into coating film during diffusion annealing, the incorporation effect was examined on $Al_2O_3$ coating film doped with $Y_2O_3$ or La. The doping was made by sputtering simultaneously $Al_2O_3$ and $Y_2O_3$ or La in a similar manner as in Section 5.2.

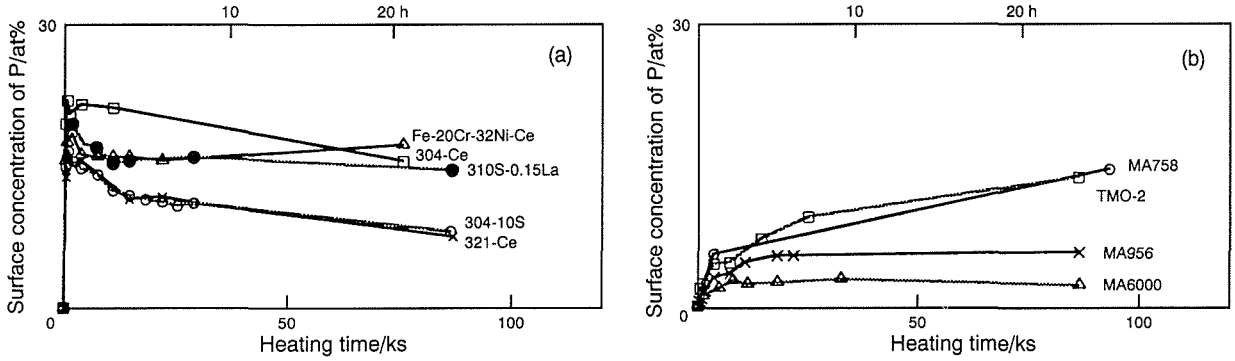


**Fig. 41 Surface segregation of P at 1100 K on various alloys where S segregation is suppressed—(a) REM addition or low S steels and (b) ODS alloys**

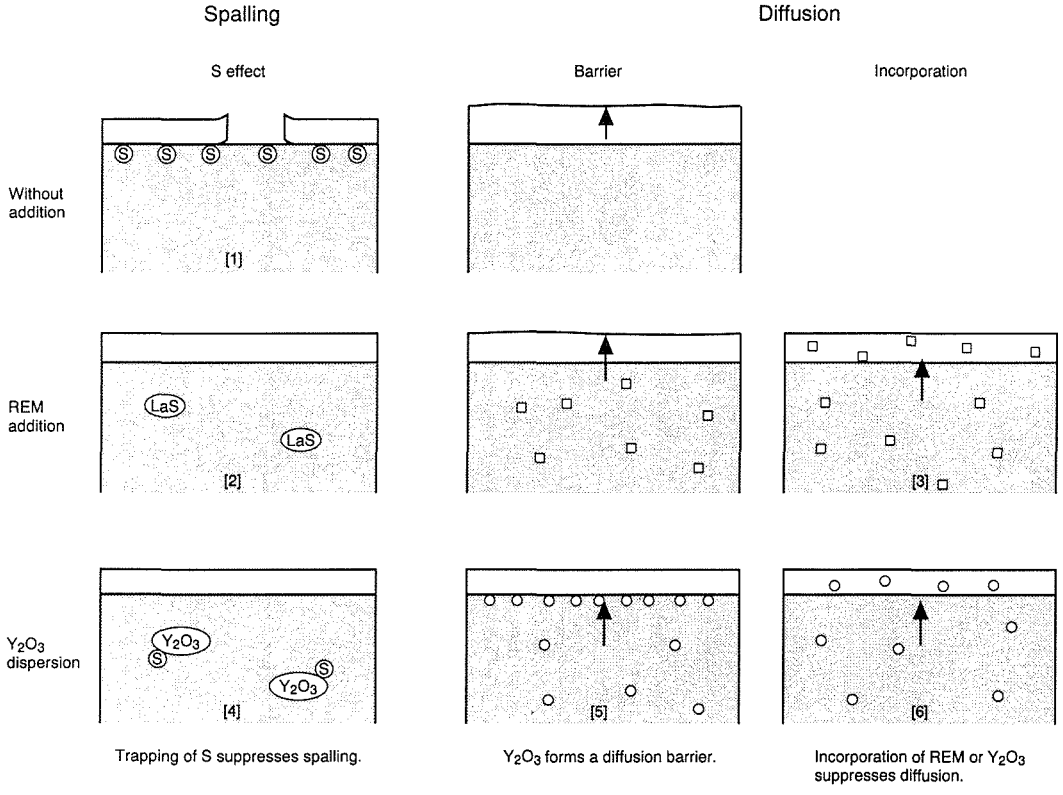


**Fig. 42 Schematic presentation of important conclusions in this work**

Type 310S and 321 steels, chosen as a substrate, were coated with $Al_2O_3$ with and without doping, and diffusion-annealed in $O_2$ for 86.4 ks (24 h) at 1200 K. Concentration profiles were taken on the cross-section and represented in Figs. 38 and 39. It is seen that La, as well as $Y_2O_3$, suppress the diffusion of alloying elements in $Al_2O_3$ film doped with them. It is reported that reactive elements incorporation during high temperature oxidation changes dominant diffusion species from cation to anion. The simulation experiment using $Al_2O_3$ coating film gives direct evidence of cationic diffusion retardation by incorporated reactive elements, supporting previously reported results[26].

## 10. Other Interesting Results Concerning $Y_2O_3$ Dispersion

### 10.1 Effect of $Y_2O_3$ on Fatigue Crack Propagation[29]

Fatigue crack propagation at high temperature will be moderated by an oxide film formed at the crack tips. If the oxide film is broken, the moderating effect will be lost. From this aspect $Y_2O_3$ is expected to moderate fatigue crack propagation through suppressing oxide cracking as shown in Figs. 29 and 30. Thus fatigue test was made on the same series of alloys as Figs. 29 and 30. The threshold $\Delta K_{eff}$ value for crack propagation was found to increase largely by $Y_2O_3$ (Fig. 40). This effect is attributable to the suppression of oxide film cracking by $Y_2O_3$. Orowan mechanism can be rejected because dispersed oxide other than $Y_2O_3$ had not any effect on the threshold value.

### 10.2 Surface Segregation of P[20]

Although surface segregation rate of P is very rapid, P is generally replaced by S in a short time. However, P survives at the surface for a long time, when S segregation is suppressed through REM addition or lowering S level (Fig. 41(a)). In contrast with REM, P segregation is fairly suppressed on ODS alloys (Fig. 41(b)). It is seen that $Y_2O_3$ can trap both S and P while REM traps S only. From the viewpoint of spalling P segregation is not so serious, for the spalling is well suppressed on alloys examined in Fig. 40(a) (Figs. 8, 10 and 12). But $Y_2O_3$ possibly suppresses the embrittlement by grain boundary segregation of P through trapping it. In any way the effect for P is one of remarkable differences between REM and $Y_2O_3$.

## 11. Conclusions

The important conclusions are presented schematically in Fig. 42. Number in brackets [ ] refers to the corresponding illustration in the Figure.

1) S promotes the spalling of protective film through weakening the bond between the film and substrate alloy (Fig. 42[**1**]).
2) REM addition affords excellent resistance to high temperature oxidation through trapping S [**2**], and additionally suppressing the diffusion of alloying elements in protective film if REM is incorporated in the film [**3**].
3) $Y_2O_3$ dispersion affords excellent resistance to high temperature oxidation through trapping S [**4**], additionally forming a diffusion barrier [**5**] and suppressing the diffusion of alloying elements in protective film [**6**], and probably by other minor effects.
4) $Y_2O_3$ is superior to REMs and other oxides in suppressing the diffusion, improving fatigue properties, suppressing P segregation, etc.
5) Mechanical alloying can afford more excellent oxidation resistance than casting.
6) $Y_2O_3$-alloy composite spray coating can be used instead of mechanical alloying for oxidation protection.
7) Simulation experiment using oxide coating film is powerful in elucidating separately several factors controlling high temperature oxidation.

## Acknowledgements

Special acknowledgment is made of the discussion and assistance rendered by Director General Dr. K. Nii and every member in NRIM. The author is grateful also for preparing the samples to Dr. T. Yamazaki, Dr. H. Fujikawa, Mr. Y. Ishiwata, Dr. T. Iikubo and Nara machinery Co., Ltd.

## References

1) Y. Ikeda, K. Nii and K. Yoshihara: Proc. 3rd. JIM Int. Symp. on High Temperature Corrosion of Metals and Alloys, Suppl. to Trans. Jpn. Inst. Met., **24** (1983), 207.
2) J.G. Smeggil, A.W. Funkenbusch and N.S. Bornstein: Metall. Trans. A, **17A** (1986), 923.
3) D.G. Lees: Oxid. Met., **27** (1987), 75.
4) J.L. Smialek: Metall. Trans. A, **18A** (1987), 164.
5) D.R. Sigler: Oxid. Met., **29** (1988), 23.
6) I. Melas and D.G. Lees: Mater. Sci. Tech., **4** (1988), 455.
7) P. Fox, D.G. Lees and G.W. Lorimer: Oxid. Met., **36** (1991), 491.

8) K.L. Ruthra and C.L. Briant: Oxid. Met., **26** (1986), 397.
9) Y. Ikeda, M. Tosa, K. Yoshihara and K. Nii: ISIJ Int., **29** (1989), 966.
10) Y. Ikeda and M. Yata: ISIJ Int., **31** (1991), 750.
11) Y. Ikeda, K. Nii and M. Yata: ISIJ Int., **33** (1993), 298.
12) H. Nagai and Y. Takebayashi: J. Jpn. Powder and Powder Metall., **29** (1982), 95 (in Japanese).
13) Y. Ikeda, H. Sumiyoshi, S. Matsuoka and E. Takeuchi: Proc. 2nd Int. Conf. on Mechanical Alloying for Structural Applications, Vancouver, ed. ASM Int., **125** (1993).
14) P.Y. Hou and J. Stringer: Oxid. Met., **38** (1992), 323.
15) Y. Ikeda, M. Yoshitake, K. Yoshihara and K. Nii: ISIJ Int., **31** (1991), 162.
16) L.E. Davis, N.C. MacDonald, P.W. Palmberg, G.E. Riach and R.E. Weber: "Handbook of Auger Electron Spectroscopy." 2nd. ed., Perkin-Elmer Corp., Eden Prairie, MN, (1978).
17) M. Tosa, K. Yoshihara and K. Nii: J. Jpn. Inst. Met., **50** (1986), 915 (in Japanese).
18) Y. Ikeda, M. Tosa, K. Yoshihara and K. Nii: J. Jpn. Inst. Met., **51** (1987), 839 (in Japanese).
19) D. Delaunay and A.M. Huntz: J. Mat. Sci., **17** (1982), 2027.
20) Y. Ikeda, H. Sumiyoshi and Y. Ishiwata: ISIJ Int., **35** (1995), to be published.
21) G.V. Samsonov: "Oxides Data Book—Physical and Chemical Properties"—2nd ed. (Translation in Japanese, ed. by Jpn. Casting and Forging Soc., Osaka, (1978), 126.
22) Jpn. Inst. Met.: "Metals Data Book," 2nd ed., Maruzen, Tokyo, (1984), 116 (in Japanese).
23) IncoMAP publication PP-1, Physical Properties INCOLOY alloy MA965.
24) INCO ALLOYS INTERNATIONAL publication 2M 8–88 IAI-51, INCONEL alloy MA6000.
25) H. Sumiyoshi, Y. Ikeda and H. Masuda: J. Jpn. Inst. Met., to be published.
26) W.J. Quadakkers, H. Halzbrechen, K.G. Brief and H. Beske: Oxid. Met., **32** (1989), 67.
27) Y. Ikeda and N. Washizu: Defect and Diffusion Forum, **95–98** (1993), 1089.
28) R. Prescott and M.J. Graham: Oxid. Met., **38** (1992), 233.
29) E. Takeuchi, S. Matsuoka, K. Miyahara, H. Hirukawa and Y. Ikeda: Trans. JSME, **60** (1994), 1487 (in Japanese).

Effect of S, REM and $Y_2O_3$ on High Temperature Protective Film

by

Yuji IKEDA

NRIM Special Report
(Research Report)
No. 95-02

Date of issue: 31 March, 1995

---



---

Publisher, Contact:
Toshikazu ISHII
Planning Office
National Research Institute for Metals
1–2–1, Sengen, Tsukuba-shi, Ibaraki 305, Japan
Phone: +81-298-53-1045 Fax: +81-298-53-1005

---



---

Typeset using the SGML by Uniscope, Inc., Tokyo

# Effect of S, REM and $Y_2O_3$ on High Temperature Protective Film

by
Yuji IKEDA

NRIM Special Report
(Research Report)
No. 95–02

## Contents